JBC Paper in Press
Published on May 8, 2020 as Manuscript RA119.011650
Latest version at https://www.jbc.org/cgi/doi/10.1074/jbc.RA119.011650

Intramitochondrial proteostasis is directly coupled to α-synuclein and amyloid β 1-42 pathologies

Janin Lautenschläger[1*], Sara Wagner-Valladolid[1], Amberley D. Stephens[1], Ana Fernández-Villegas[1], Colin Hockings[1], Ajay Mishra[1], James D. Manton[2], Marcus J. Fantham[3], Meng Lu[1], Eric J. Rees[2], Clemens F. Kaminski[3], Gabriele S. Kaminski Schierle[1*]

[1] Molecular Neuroscience Group, Department of Chemical Engineering and Biotechnology, University of Cambridge, West Cambridge Site, Philippa Fawcett Drive, Cambridge, CB3 0AS, UK; [2] Quantitative Imaging Group, Department of Chemical Engineering and Biotechnology, University of Cambridge, West Cambridge Site, Philippa Fawcett Drive, Cambridge, CB3 0AS, UK; [3] Laser Analytics Group, Department of Chemical Engineering and Biotechnology, University of Cambridge, West Cambridge Site, Philippa Fawcett Drive, Cambridge, CB3 0AS, UK

* Corresponding authors:
Janin Lautenschläger, Gabriele S. Kaminski Schierle
Email: janin.lautenschlaeger@gmail.com, gsk20@cam.ac.uk
Molecular Neuroscience Group, Department of Chemical Engineering and Biotechnology
University of Cambridge, West Cambridge Site, Philippa Fawcett Drive, Cambridge, CB3 0AS, UK

Running title: Intramitochondrial proteostasisis and α-syn/Aβ42 pathologies

Keywords: alpha-synuclein; amyloid-beta (Aβ); mitochondria; neurodegeneration; HtrA2/Omi; HtrA serine peptidase 2; Parkinson disease; protein aggregation; protein homeostasis; Lon protease; Lon peptidase 1 mitochondrial

Abstract

Mitochondrial dysfunction has long been implicated in the neurodegenerative disorder Parkinson's disease (PD); however, it is unclear how mitochondrial impairment and α-synuclein pathology are coupled. Using specific mitochondrial inhibitors, EM analysis, and biochemical assays, we report here that intramitochondrial protein homeostasis plays a major role in α-synuclein aggregation. We found that interference with intramitochondrial proteases, such as HtrA2 and Lon protease, and mitochondrial protein import significantly aggravates α-synuclein seeding. In contrast, direct inhibition of mitochondrial complex I, an increase in intracellular calcium concentration, or formation of reactive oxygen species (ROS), all of which have been associated with mitochondrial stress, did not affect α-synuclein pathology. We further demonstrate that similar mechanisms are involved in amyloid β 1-42 (Aβ42) aggregation. Our results suggest that, in addition to other protein quality-control pathways such as the ubiquitin–proteasome system, mitochondria per se can influence protein homeostasis of cytosolic aggregation-prone proteins. We propose that approaches that seek to maintain mitochondrial fitness, rather than target downstream mitochondrial dysfunction, may aid in the search for therapeutic strategies to manage PD and related neuropathologies.

Introduction

Parkinson's disease (PD) is the second most common neurodegenerative disease and affects about 1% of the population over 60 years (1). Alpha-synuclein aggregation has been found central to the disease, since SNCA mutations are associated with familiar PD (2) and alpha-synuclein has been identified as a major constituent of Lewy bodies in sporadic PD and dementia with Lewy bodies (3). The relationship between protein aggregation and protein levels is well established in cases of familiar PD involving SNCA gene duplication and triplication (4–6), however what triggers protein aggregation in sporadic cases of PD is less clear. Likewise, Alzheimer's disease is linked to increased protein aggregation, where enhanced levels of Amyloid beta (Aβ) due to mutations in the genes coding for the amyloid precursor protein (APP) (7, 8) or presenilin (9–11) are found in familiar AD.

Mitochondria have long been implicated in PD, ever since the discovery that inhibitors of the mitochondrial complex I can lead to dopaminergic neuron death (12–16). Furthermore, the regulation of mitophagy via the PTEN-induced kinase 1 (PINK1) plays a role in PD (17) and seems to be coupled to alpha-synuclein toxicity. PINK1 overexpression is able to decrease the effect of alpha-synuclein toxicity in Drosophila (18, 19), and PINK1 knockout in mice increases alpha-synuclein neurotoxicity (20, 21). Furthermore, PINK1 iPSC-derived midbrain dopaminergic neurons show accumulation and aggregation of alpha-synuclein (22), and PINK1 knockout rats display alpha-synuclein de novo aggregation (23).

We have demonstrated previously that alpha-synuclein interaction with calcium leads to conformational changes at the C-terminus of alpha-synuclein, but also at the aggregation-prone non-amyloid component (NAC)-region, suggesting that calcium can directly influence the aggregation propensity of alpha-synuclein (24). Thus, we tested, whether treatment with BAPTA-AM, which is supposed to decrease intracellular calcium by calcium chelation, was able to decrease alpha-synuclein pathology. Surprisingly, prolonged incubation with BAPTA-AM significantly enhanced alpha-synuclein aggregation. We could show that BAPTA-AM treatment was accompanied by mitochondrial fragmentation, which led us to study and show that disturbances in intra-mitochondrial proteostasis could aggravate alpha-synuclein aggregation. We identified that the Lon protease and the high-temperature requirement protein A2 (HtrA2) protease, as well as mitochondrial protein import were crucial in determining the level of alpha-synuclein aggregation. However, inhibition of the mitochondrial complex I and a direct increase in cytosolic calcium or oxidative stress were not able to increase alpha-synuclein aggregation after seeding to a similar extent such as observed upon inhibition of mitochondrial protein homeostasis. In addition, inhibition of the mitochondrial protease HtrA2 and blocking mitochondrial protein import also increased Aβ42 aggregation and we could show

that isolated mitochondria were directly capable to diminish Aβ42 aggregation in-vitro.

Results

Prolonged BAPTA-AM treatment of cells increases alpha-synuclein pathology

SH-SY5Y cells overexpressing YFP-alpha-synuclein were incubated for 4 hours (h) with small fibrillar seeds made of unlabelled human recombinant alpha-synuclein to study alpha-synuclein pathology after seeding, as described previously (25–29). Cells were left in culture for 3 days before the level of alpha-synuclein aggregation within the cells was determined (see Supplementary Fig. 1A and B for treatment regime and fibrillar seeds). While unseeded YFP-alpha-synuclein overexpressing cells did not display any aggregates, those that were seeded displayed large YFP-alpha-synuclein-positive aggregates which were built up from fine filaments (Supplementary Fig. 1C). Furthermore, YFP-alpha-synuclein inclusions stained positive for ubiquitin and p62, which are both characteristic markers of Lewy bodies in human disease (25) (Supplementary Fig. 1D and E).

We have previously shown that alpha-synuclein strongly interacts with calcium, leading to conformational changes both at the C-terminal calcium-binding domain, and the aggregation-prone non-amyloid component (NAC)-region, which suggests that calcium can directly influence the aggregation propensity of alpha-synuclein. Consistently, increased calcium concentrations significantly enhanced alpha-synuclein nucleation in-vitro (24). BAPTA-AM, a calcium chelator, is supposed to decrease cytosolic calcium and has previously been reported to alleviate KCl-induced alpha-synuclein aggregation (30). However, when we treated the above-described cells with BAPTA-AM before the incubation with fibrillary seeds (1h) or before and during incubation with fibrillary seeds (5h), alpha-synuclein aggregation was drastically increased (Fig. 1A). We thus tested the calcium effect of BAPTA-AM in SH-SY5Y cells and verified that BAPTA-AM was able to decrease cytosolic calcium. However, the calcium buffering achieved by BAPTA-AM was only transient and cytosolic calcium concentrations were already back to control levels after longer treatment with BAPTA-AM, which is due to the cells compensating for reduced calcium levels (Fig. 1B, fluorescence lifetime decrease after 10 min from 2381+/-8 ps to 2170+/-15 ps, $p < 0.0001$, lifetime of 2400 +/-8 ps after 1h and 2460+/-12 ps after 5h). Since the 1 h treatment of cells with BAPTA-AM led to calcium levels comparable to control but already to increased alpha-synuclein aggregation suggested that the increase of alpha-synuclein aggregation by BAPTA-AM was not directly mediated by increased intracellular calcium concentrations. In addition, we tested whether both the ester form of BAPTA, BAPTA-AM, as well as the active BAPTA itself were directly capable to affect the aggregation of alpha-synuclein. We found no difference in alpha-synuclein aggregation kinetics measured in-vitro by Thioflavin T (ThT) fluorescence in the presence of BAPTA and BAPTA-AM (Fig. 1C, t_{50} 125.6+/-8.6 h and 122.6+/-7.2 h vs. 116.6+/-11.1 h) confirming that the effect of BAPTA is most likely triggered by a cellular response. We consequently discovered a previous publication showing that BAPTA-AM could lead to mitochondrial fragmentation (31). We thus stained the cells with Mitochondria-RFP, a mitochondrial marker, and showed that prolonged BAPTA-AM treatment of cells led to mitochondrial fragmentation (Fig. 1D).

Thus, we hypothesized that mitochondrial dysfunction may influence alpha-synuclein aggregation per se, which we tested by treating cells with carbonyl cyanide 4-(trifluoromethoxy)phenylhydrazone (FCCP), a mitochondrial uncoupler which dissipates the mitochondrial membrane potential. Treatment of cells with FCCP during alpha-synuclein fibril incubation (5h) significantly increased alpha-synuclein aggregation (Fig. 1E). In order to test whether FCCP did not increase alpha-synuclein aggregation per se, we also performed an in-vitro aggregation assay and showed that FCCP was not capable to influence alpha-synuclein aggregation directly (t_{50} 117.0+/-9.8 h vs. 115.6+/-10.1 h). We thus confirmed that the effect of FCCP treatment in cells is the result of a cellular response rather than of a direct interaction of FCCP with alpha-synuclein (Fig.1F).

Classical downstream effectors of mitochondrial dysfunction are unable to influence alpha-synuclein pathology

We next tested whether downstream events of mitochondrial dysfunction could reproduce increased alpha-synuclein aggregation. We therefore used 1-methyl-4-phenylpyridinium (MPP^+), the active metabolite of 1-methyl-4-phenyl-1,2,3,6-tetrahydropyridine (MPTP) to inhibit complex I of the electron transport chain, therewith inhibiting mitochondrial ATP production. We used ionomycin, an ionophore, to directly increase cytosolic calcium concentrations via calcium influx through the plasma membrane, and we used menadione to induce the formation of reactive oxygen species (ROS) via redox-cycling (32). However, when YFP-alpha-synuclein overexpressing SH-SY5Y cells with alpha-synuclein seeds were treated for 3 days, no increase in alpha-synuclein aggregation could be detected (Fig. 2A). To test that the various inhibitors were active, we measured ATP, calcium and H_2O_2 levels in SH-SY5Y cells using the fluorescent sensors Ateam1.03 (33, 34), Oregon-Green™ BAPTA-1 and HyPer (35) respectively. The readout of the fluorescence lifetime of these sensors permits to estimate and directly compare the effect of our different treatments (36, 37). Our results show that MPP^+-induced inhibition of complex I reduced ATP levels (Fig. 2B, fluorescence lifetime increase of the FRET donor from 1298 +/- 17 ps to 1511 +/- 20 ps, $p < 0.0001$), ionomycin treatment of cells increased cytosolic calcium concentrations (Fig. 2C, fluorescence lifetime increase of Oregon-Green™ BAPTA-1 from 2381 +/- 8 ps to 2663 +/- 7 ps, $p < 0.0001$), and menadione treatment increased H_2O_2 levels in cells (Fig. 2D, fluorescence lifetime decrease of cpYFP from 1575 +/- 4 ps to 1557 +/- 3 ps, $p = 0.0017$). Treatment of cells with MPP^+ lead to less ATP depletion than treatment of cells with FCCP, but to higher ATP depletion than following BAPTA-AM treatment (Fig. 2B). Ionomycin treatment led to a higher calcium increase compared to both, FCCP and BAPTA-AM treatment (Fig 2C). Moreover, menadione treatment of cells led to a comparable increase in H_2O_2 concentrations than treatment with FCCP and BAPTA-AM (Fig. 2D). In summary, the above experiments shown that there is no correlation between a loss in ATP-levels, an increase in calcium or H_2O_2 concentrations and increased alpha-synuclein pathology.

Inhibition of mitochondrial proteostasis increases alpha-synuclein pathology

In the next step, we evaluated the level of mitochondrial fragmentation upon treatment with FCCP and BAPTA-AM, as well as MPP^+, ionomycin and menadione. Automated analysis of mitochondrial length showed that both FCCP and BAPTA-AM treatment led to mitochondrial fragmentation, while neither MPP^+, nor ionomycin or menadione did (Fig. 3A and B). Furthermore, we saw that FCCP treatment led to higher levels of mitochondrial fragmentation compared to BAPTA-AM, though the effect of BAPTA-AM on alpha-synuclein aggregation was more pronounced than upon FCCP treatment (refer to Fig. 1A and E), suggesting that additional factors might play a role at increasing alpha-synuclein aggregation.

Previously, it has been reported that BAPTA-AM can inhibit proteases (38–40), which is mediated via blocking intracellular calcium transients required to regulate protease activity (41, 42). This led us to test the effect of mitochondrial proteostasis on alpha-synuclein pathology. We treated YFP-alpha-synuclein overexpressing SH-SY5Y cells with CDDO-Me to inhibit Lon protease (43), which has recently been shown to influence aggregate dissolution after heat shock (44), and with UCF-101 to inhibit high temperature requirement protein A2 (HtrA2/Omi) protease (45), which has previously been linked to PD. Our results show that both mitochondrial protease inhibitors significantly increase alpha-synuclein pathology (Fig. 3C), with the effect of HtrA2 protease inhibition on aggregation being higher than the one of Lon protease inhibition.

Inhibition of mitochondrial proteostasis increases Amyloid β 1-42 pathology

To test if the above-discussed mechanisms also contribute to the aggregation of other proteins involved in neurodegeneration, we investigated the effect of mitochondrial proteostasis on Amyloid β 1-42 (Aβ42) aggregation. We used a stable HEK293 cell line overexpressing Aβ42-mCherry via a tetracycline-inducible expression system which is described in detail in (46).

After induction of Aβ42-mCherry expression, the cells were treated with FCCP, BAPTA-AM and the protease inhibitors CDDO-Me and UCF-101. We found that treatment of cells with both, FCCP and BAPTA-AM, increased the aggregation of Aβ42 (Fig. 4A). BAPTA-AM had a more pronounced effect to enhance Aβ42 aggregation compared to FCCP, similar to what had been seen for alpha-synuclein. Inhibition of the Lon protease did not significantly increase Aβ42 aggregation, however inhibition of HtrA2 using UCF-101 again increased Aβ42 aggregation (Fig. 4B). To test whether increased mitochondrial proteostasis via HtrA2 is indeed able to influence protein aggregation we overexpressed HtrA2 in Aβ42-mCherry HEK cells. After transfection of the cells with HtrA2 and 3 days of induction of Aβ42-mCherry expression we observed a significant reduction of Aβ42 aggregation (Fig. 4C).

In-vitro aggregation of Amyloid β 1-42 is influenced by mitochondria and HtrA2

In order to show that mitochondria directly influence protein homeostasis, we chose to investigate Aβ42 aggregation in-vitro using a fluorescence lifetime aggregation assay. While alpha-synuclein aggregation occurs within days (see ThT assays in Fig 1C and F), Aβ42 shows very fast aggregation kinetics (within hours), which permitted us to investigate the effect of isolated brain mitochondria (viable for only several hours). The fluorescence lifetime assay we have used analyses the reduction in fluorescence lifetime of labelled proteins when they start to aggregate and are tightly packed, as previously described in detail (47, 48). We used Aβ42 containing 50 % Hylite^{TM} Fluor 488 labelled Aβ42 which was incubated for 2h at room temperature, after which we measured a reduction of Hylite^{TM} Fluor 488 fluorescence lifetime from 3380 +/- 93 ps to 3003 +/- 97 ps (Fig. 5A control t0 and t2h). However, in the presence of isolated rat brain mitochondria, only a small drop in Aβ42 Hylite^{TM} Fluor 488 fluorescence lifetime was detected (Fig. 5A mito t0 and t2h, 3538 +/- 15 ps compared to 3502 +/- 5 ps). Note, the fluorescence lifetime of Aβ42 Hylite^{TM} Fluor 488 incubated with mitochondria is higher at the beginning of the experiment (t0) than in the control group (Aβ42 + mito 3538 +/- 15 ps vs. Aβ42 control with 3380 +/- 93 ps), since in the control Aβ42 starts to aggregate immediately upon preparation which was not the case in the presence of mitochondria. We next pre-incubated mitochondria with UCF-101 and showed that the Aβ42 Hylite^{TM} Fluor 488 fluorescence lifetime significantly decreased over the 2h time interval, demonstrating that Aβ42 aggregation was increased upon inhibition of HtrA2 (Fig. 5B, UCF-101 t0 and t2h, 3523 +/- 16 ps vs. 3429 +/- 20 ps).

Inhibition of mitochondrial protein import enhances alpha-synuclein and Amyloid β 1-42 pathology

There is recent evidence in the literature that mitochondrial proteases can influence aggregate dissolution and that aggregation-prone proteins are directed to mitochondrial import (44). There is one report showing mitochondrial import of alpha-synuclein (49), but it is still discussed critically that aggregation-prone proteins like alpha-synuclein are directly imported into mitochondria (50, 51). Thus, in order to prove that alpha-synuclein resides within mitochondria, we immuno-gold labelled YFP-alpha-synuclein in SH-SY5Y cells, and found specific staining within mitochondria, which was mainly located at the inner mitochondrial membrane (Fig. 6A and Supplementary Fig. 2). In addition, we isolated mitochondria from wild-type adult rat brain and probed them for the presence of endogenous alpha-synuclein after protein K (PK) digestion. We see that alpha-synuclein is still present after PK treatment, indicating that alpha-synuclein resides within the organelle since PK is not able to degrade proteins protected by organelle membranes. This is further supported by the finding that incubation with 0.1% Triton X-100 during PK treatment, which is capable to solubilize mitochondrial membranes (52), enables complete alpha-synuclein degradation (Fig. 6B and C).

Since the above results indicated that alpha-synuclein was localized to mitochondria, we hypothesized that inhibition of mitochondrial protein import might have a similar effect on alpha-synuclein pathology as the inhibition of proteases. Thus, using MitobloCK-6, a small molecule inhibitor of protein translocation into mitochondria (53), we also observed increased alpha-synuclein aggregation in YFP-alpha-

synuclein overexpressing SH-SY5Y cells (Fig. 6D). Testing MitobloCK-6 on Aβ42-mCherry overexpressing HEK cells again showed increased Aβ42 aggregation (Fig. 6E), demonstrating that mitochondrial protein import influences the proteostasis of amyloidogenic proteins.

To test how cytosolic protein homeostasis is influenced by other protein quality control pathways, we used Aβ42-mCherry overexpressing HEK cells and inhibited autophagy using bafilomycin A1, the ubiquitin-proteasome system (UPS) using MG132 and the cytosolic chaperone Hsp90 using 17-AAG. While bafilomycin A1 and 17-AAG did not increase Aβ42 aggregation, inhibition of the UPS using MG132 increased the aggregation of Aβ42 (Fig. 6F), which is in accordance with previous reports (54–56).

Discussion

We demonstrate here that inhibition of the mitochondrial proteases HtrA2 and Lon, as well as inhibition of mitochondrial protein import enhances alpha-synuclein pathology. However, downstream effects of mitochondrial dysfunction, induced without effects on the mitochondrial network, did not recapitulate increased alpha-synuclein pathology. Inhibition of HtrA2 and of mitochondrial protein import further increased Aβ42 pathology, and overexpression of HtrA2 was able to decrease Aβ42 aggregation notably. It was reported recently that mitochondria were able to influence the degradation and protein homeostasis of cytosolic proteins, which has been shown in yeast cells upon heat shock (44). Mitochondria may also play an important role for the degradation of amyloidogenic proteins, since mitochondrial proteostasis seems to be clearly coupled to the pathology of alpha-synuclein and Aβ42. HtrA2 appears of particular interest, since it has previously been linked genetically to PD (57–61) and shows a neuroprotective effect upon overexpression in mice (62, 63).

So far the effect of amyloid proteins on mitochondria has been interpreted only as a secondary pathological hallmark, with alpha-synuclein as well as Aβ exacerbating mitochondrial dysfunction (50, 51, 64–68). However, amyloidogenic proteins may be deliberately directed to mitochondria, and thereby disrupt overall mitochondrial function if uptake is overloaded. Vice versa, an initial failure in mitochondrial function, i.e. by severe complex I inhibition or upon disturbance of mitophagy, can eventually lead to increased levels of alpha-synuclein, having important implications for sporadic forms of the disease. Our recently published review provides more insight into mitochondrial uptake of alpha-synuclein and Aβ, on the interaction with mitochondrial translocases as well as background information on mitochondrial proteases (69). In addition to what is already known, our study here shows that mitochondrial proteostasis can influence the aggregation of alpha-synuclein after seeding. Thus far, it has only been shown that alpha-synuclein is taken up into mitochondria (49), but not that intra-mitochondrial proteases influence alpha-synuclein aggregation propensity. Furthermore, our findings are from an alpha-synuclein seeding model. This is especially important, since seeding is understood as a major mechanism during the progression of PD and thus targeting mitochondrial proteostasis in patients may thus be a promising approach to tackle PD. For Aβ, several studies, especially from the lab of Elzbieta Glaser, show that Aβ can be taken up into mitochondria and that mitochondrial proteases can influence protein aggregation (70–72). Here we present new data on HtrA2 and add further evidence that mitochondrial proteostasis is indeed of physiological and pathophysiological relevance for neurodegenerative diseases.

There still remains the argument that inhibition of mitochondrial proteases just causes unspecific mitochondrial dysfunction which then per se leads to increased alpha-synuclein aggregation. However, it seems that this effect is not mediated via the known downstream events of mitochondrial dysfunction. Indeed, ATP depletion is not able to increase alpha-synuclein aggregation, as seen in our study using short term complex I inhibition via MPP^+ (where MPP^+ reduced ATP levels, but did not lead to major mitochondrial fragmentation). Furthermore, a previous study shows that there is no elevated toxicity when ATP levels are reduced independently from mitochondrial respiration using 2-Desoxyglucose, which inhibits cytosolic glycolysis (73). Furthermore,

increased calcium concentrations, when induced acutely via calcium influx through the plasma membrane using the ionophore ionomycin, did not influence alpha-synuclein aggregation after seeding. This, in the first instance, seems to stand in contrast to our previous study (24), where we have shown that calcium affects alpha-synuclein aggregation in-vitro. However, we saw that mainly the nucleation rate was increased, thus how fast new aggregates are formed, but not the growth rate, i.e. how fast aggregates grow from an existing seed. Taken together this implies that calcium may contribute to PD via alpha-synuclein seed formation, but less to the growth from already formed alpha-synuclein seeds. Oxidative stress has been discussed as a likely mechanism in PD, since antioxidants are able to reduce dopaminergic neuron death and alpha-synuclein accumulation after complex I inhibition (73), however also a general protective impact on mitochondria may play a role.

Though, this does not mean that complex I inhibition, calcium dysregulation and oxidative stress are not important during the course of the disease. Chronic complex I inhibition has clearly been shown to lead to dopaminergic neuron death and alpha-synuclein accumulation (12–16) and is a major factor implicating mitochondrial dysfunction in sporadic Parkinson's disease. Chronic complex I inhibition can impact mitochondrial fitness. And mitochondrial fitness can also be reduced upon high calcium loads as recently demonstrated for dopaminergic neurons of the substantia nigra (74). Taken together, our study shows that mitochondrial proteostasis may be an important factor contributing to the pathology of neurodegenerative diseases, and attacking mitochondrial fitness, rather than downstream events of mitochondrial dysfunction may be crucial in the search for therapeutic strategies.

Experimental Procedures

Human cell cultures

Human neuroblastoma cells (SH-SY5Y) were obtained from the European Collection of Cell Cultures (ECACC, Sigma-Aldrich, Dorset, UK) and grown in a 1:1 minimal essential medium (MEM) (Sigma-Aldrich) and nutrient mixture F-12 Ham (Sigma-Aldrich) supplemented with 15 % FBS, 1 % non-essential amino acids, 2 mM GlutaMAX and 1 % antibiotic-antimycotic (all Thermo Fisher Scientific, Epsom, UK). SH-SY5Y cells stably expressing YFP-alpha-synuclein were obtained by lentiviral transfection using 3rd generation lentiviruses (Addgene constructs: 12251, 12253, 12259). pMDLg/pRRE, pRSV-Rev and pMD2.G was a gift from Didier Trono (Addgene plasmid # 12251, # 12253 and # 12259; http://n2t.net/addgene:12251 ; RRID:Addgene_12251, http://n2t.net/addgene:12253 ; RRID:Addgene_12253 and http://n2t.net/addgene:12259 ; RRID:Addgene_12259) (75). Human wild-type alpha-synuclein was inserted into EYFP plasmid (pEYFP-N1) using a 5 amino acid linker (sequence: GCACCGGTCGCCACC) between the C-terminus of alpha-synuclein and N-terminal EYFP. Alpha-synuclein-EYFP was then cloned into the pLJM1 backbone for lentiviral expression (Addgene: 19319). pLJM1-EGFP was a gift from David Sabatini (Addgene plasmid # 19319 ; http://n2t.net/addgene:19319 ; RRID:Addgene_19319) (76). For the preformed fibril (PFF) assay, 50,000 cells were plated in MatTek dishes (P35G-1.5-14-C, MatTek Corporation, Ashland, US). For analysis of mitochondrial fragmentation cells were plated at 20,000 cells per well in NuncTM Lab-TekTM II Chambered Coverglass (8 well, 155409, Thermo Fisher Scientific).

Flp-InTM T-RExTM 293 cell line (Invitrogen), a derivative of HEK293 cells containing a stably integrated FRT site and a TetR repressor, was used to generate stable cell lines expressing either mCherry or Aβ42-mCherry (pcDNA3.3-mCherry, pcDNA3.3-Ab42-mCherry) under the Flp-InTM expression vector as described previously (46, 77). Cells were maintained in DMEM high glucose media (Sigma-Aldrich) supplemented with 10% fetal bovine serum (FBS), 2 mM glutaMAX, and 1 % antibiotic-antimycotic (all Thermo Fisher Scientific). Cells were grown at 37°C under a 5% CO_2 atmosphere. Cells were plated at 35 000 cells per well in NUNC 24 well plates, and construct expression was induced for 3 days using media above with 1 µg/mL tetracycline (Sigma Aldrich) added. All cell lines were tested for mycoplasma contamination using the MycoAlert^{TM} PLUS mycoplasma detection kit (Lonza, Walkersville). For transient

transfection of HtrA2 electroporation with the NEON transfection system was used (settings: 1050 V, 30 ms, 2 pulses; Thermo Fisher Scientific). pcDNA3-HtrA2-FLAG was a gift from L. Miguel Martins (Addgene plasmid # 15938; http://n2t.net/addgene:15938; RRID:Addgene_15938) (78).

Cells were imaged on a widefield microscope with IX83 frame (Olympus, Tokyo, Japan), HPLS343 plasma light source (Thorlabs, Newton, US), and Clara interline CCD camera (Andor, Belfast, UK), controlled by Micromanager (79). Respective filter cubes for YFP (excitation 500 nm, dichroic mirror 515 nm, emission 535 nm), RFP (excitation 560 nm, dichroic mirror 585 nm, emission 630 nm) and DAPI (excitation 350 nm, dichroic mirror 400 nm, emission 460 nm) were used. Images for YFP-alpha-synuclein aggregation and DAPI were taken with an Olympus Plan Apo U 60x/1.42 oil objective lens. Imaging was done randomly by automated acquisition of a grid of 7x7 images per area. Aggregates were identified by their fibrillar nature, cell nuclei were counted using FIJI (80). For Aβ42-mCherry aggregation images were taken with an Olympus LUCPlanFLN 20x/0.45 air objective lens. Aggregates were identified using the Thresholder plugin in ICY (81). The cell surface area was evaluated using the HK-Means plugin for ICY (82).

Alpha-synuclein fibrils

Human wild-type (WT) alpha-synuclein was expressed in Escherichia coli One Shot® BL21 STAR™ (DE3) (Invitrogen, Thermo Fisher Scientific) cells using plasmid pT7-7 and purified using ion-exchange on a HiPrep Q FF 16/10 anion exchange column (GE Healthcare, Uppsala, Sweden) (83). Alpha-synuclein was then further purified on a HiPrep Phenyl FF 16/10 (High Sub) hydrophobic interaction column (GE Healthcare) (84). Purification was performed on an ÄKTA Pure (GE Healthcare). Monomeric protein was dialysed against 20 mM phosphate buffer pH 7.2, lyophilized in a LyoQuest 85 freeze-dryer (Telstar, Spain), and stored at -80 °C.

Alpha-synuclein fibrils were produced by diluting alpha-synuclein monomer solution to a concentration of 150 µM in 20 mM phosphate buffer, pH 7.2. Samples were incubated at 37°C for 5 days in 0.5 mL Protein Lobind tubes (Eppendorf, Hamburg, Germany) under continuous rotation at maximum speed (UVP HB-1000 Hybridizer, Fisher Scientific). Fibrils were diluted 1:1 with 20 mM phosphate buffer, pH 7.2 to a final volume of 200 µL and sonicated (Digital Sonifier® SLPe, model 4C15, Branson, Danbury, USA) with six 10 sec pulses at 70 % amplitude and 10-sec pause after each sonication pulse. Sonicated fibrils were aliquoted, exposed to UV light for 30 min and frozen immediately after at -80C.

Alpha-synuclein fibrils were imaged by atomic force microscopy (AFM) (BioScope Catalyst microscope, Bruker AXS GmbH, Fitchburg, USA). Fibrils at an equivalent monomer concentration of 5 µM were deposited for 30 min on High-Performance cover glass (PN 474030-9020-000, Carl Zeiss Ltd.), cleaned for 30 min with 1M KOH (Fluka, Bucharest, Romania) and coated for 30 min with 0.01 % poly-L-Lysine beforehand (P4707, Sigma). Samples were rinsed 5 times with deionized water and dried under nitrogen flow. AFM data were acquired using PeakForce Quantitative Nanomechanical Property mapping mode with ScanAsyst-Fluid+ probes (BioScope Resolve, Bruker AXS GmbH). Images were flattened and exported using NanoScope Analysis software, version 1.8.

Preformed fibril (PFF) assay

For the induction of alpha-synuclein seeding, YFP-alpha-synuclein overexpressing SH-SY5Y cells were incubated with sonicated preformed alpha-synuclein fibrils as described by Luk et al. (25). Briefly, cells plated in MatTek dishes were washed with Neurobasal medium and subsequently changed to 500 µL Neurobasal medium supplemented with 2 % B27 and 0.5 mM GlutaMAX (all Thermo Fisher Scientific). Cells were preincubated for 1 hour, either using DMSO for control or the respective treatment (see cell treatments below). 8 µL of PFFs were diluted with 32 µL HBSS (HBSS minus calcium and magnesium, no phenol red, 14175-053, Thermo Fisher Scientific) and mixed briefly 5 times. Fibrils were added to the bottom of the BioPORTER tube (BioPORTER® Protein Delivery agent, BP502424, Gelantis, San Diego, USA), mixed 5 times and incubated for 5 min at room temperature, then vortexed for 5 sec at 600 rpm (Stuart™ Scientific SA8 vortex mixer, Sigma-Aldrich). 460 µL OptiMEM medium (Thermo Fisher Scientific) was added to the

BioPORTER tube plus the respective treatments and mixed 5 times. The PFF mixture was added dropwise to the cells, settled and then incubated for 4 hours at 37°C and 5 % CO_2. Final monomer equivalent concentration of preformed fibrils was 600 nM.

After 4 hours, cells were washed twice with 1 ml Neurobasal medium and changed subsequently to 2 mL of retinoic acid medium made of 1:1 minimal essential medium (MEM) (Sigma-Aldrich) and nutrient mixture F-12 Ham (Sigma-Aldrich) supplemented with 5 % FBS, 1 % non-essential amino acids, 2 mM GlutaMAX and 1 % antibiotic-antimycotic (all Thermo Fisher Scientific) and 1 µM retinoic acid (Sigma-Aldrich) plus treatments if indicated and incubated for another 3 days to allow aggregate formation. Cells were fixed for 10 min using 4 % formaldehyde in PBS supplemented with 4 % sucrose, 5 mM $MgCl_2$ and 10 mM EGTA, pH 7.4 (85) and stained with Hoechst 33342 (Molecular Probes, Thermo Fisher Scientific) 1:2000 in PBS for 30 min.

Cell treatment

Chemicals used for the treatment of cells were prepared as followed, with final dilution made with the respective cell culture medium. Carbonyl cyanide 4-(trifluoromethoxy)phenylhydrazone (FCCP, Abcam, Cambridge, UK) 1 mM in DMSO, N-Methyl-4-phenylpyridinium Iodide (MPP^+, Sigma-Aldrich) 10 mM in water, ionomycin (ab120370, Abcam) 10 mM and 1 mM in DMSO, 2-Deoxyglucose (Sigma-Aldrich) 0.5 M in water, menadione (Sigma-Aldrich) 1.5 mM in DMSO, BAPTA-AM (ab120503, Abcam) 2.5 mM in DMSO, BAPTA (ab144924, Abcam) 1 mM in water, CDDO-Me (Sigma-Aldrich) 1 mM in DMSO, UCF-101 (Sigma-Aldrich) 10 mM in DMSO, MitobloCK-6 (Focus Biomolecules) 5 mM in DMSO, bafilomycin A1 (Calbiochem, San Diego, US) 100 µM and 10 µM in DMSO, 17-AAG (ab141433, abcam) 5 mM and 50 µM in DMSO and MG132 (Sigma-Aldrich) 10 mM and 1 mM in DMSO.

Immunofluorescence

Cells were fixed as described above, blocking and permeabilisation were performed using 5 % donkey serum in 0.05 % Tween-20 in phosphate-buffered saline (PBS) for 1 h. Primary antibodies were incubated overnight at 4°C, followed by 5 washes with PBS. Secondary antibodies were incubated for 1 hour at room temperature, followed by 5 washes with PBS. As primary antibodies anti-Ubiquitin antibody, clone Apu2 (05-1307, 1:200, Millipore, Watford, United Kingdom), anti-Ubiquitin-binding protein p62, clone 2C11 (SQSTM1, 1:200, Abnova, Taipei, Taiwan) and anti-FLAG® M2 antibody (F1804, 1:200, Sigma-Aldrich) were used. As secondary antibodies anti-rabbit and anti-mouse Alexa Fluor®647, and anti-mouse Alexa Fluor®568 (A-21245, A-21236 and A-11031 from life technologies) were used. Samples were kept in PBS containing 5 mM sodium azide (Sigma-Aldrich).

Structured illumination microscopy (SIM)

Structured illumination images were collected on a custom-built Structured Illumination Microscopy (SIM) setup which has been described in detail (86). A 60×/1.2NA water immersion lens (UPLSAPO 60XW, Olympus) focused the structured illumination pattern onto the sample. This lens also captured the samples' fluorescence emission light before imaging onto a sCMOS camera (C11440, Hamamatsu). Laser excitation wavelengths used were 488 nm (iBEAM-SMART-488, Toptica), 561 nm (OBIS 561, Coherent), and 640 nm (MLD 640, Cobolt). Respective emission filters were BA 510-550 (Olympus), BrightLine FF01-600/37, and BrightLine FF01-676/29 (Semrock, New York, US). Imaging was done on fixed or live cells, as indicated. Images were acquired using custom SIM software (HCImage, Mamamatsu Corporation, Sewickley, US). Nine raw images were collected at each plane and each color. FairSIM plugin in FIJI was used to reconstruct images (87).

FLIM measurements of cytosolic calcium, H_2O_2, and ATP

Fluorescence lifetime microscopy (FLIM) was carried out on a custom-built Time-Correlated Single Photon Counting (TCSPC) system using a super-continuum laser (SC450, Fianium) with a pulse repetition rate of 40 MHz, a confocal

scanning unit (FluoView 300, Olympus) coupled with an inverted microscope frame (IX70, Olympus), and a time-correlated single-photon counting system (Becker & Hickl GmbH) as described in detail before (88). The excitation wavelength was selected by using an acousto-optic tunable filter (AOTFnC-400.650, Quanta Tech) and respective excitation filters (to improve the wavelength selection), and emission fluorescence was imaged through respective emission filters. The data acquisition time was 200 sec for each FLIM image (10 cycles, 20 sec per cycle). The photon detection rate was kept below 2% of the laser repetition rate in order to avoid photon pile-up.

For cytosolic calcium measurements SH-SY5Y cells were incubated with Oregon Green™ 488 BAPTA-1, AM (Thermo Fisher Scientific) for 45 min at 1 µM concentration. Excitation was set to 475 nm, excitation filter BrightLine FF01-474/27 (Semrock), and emission filter BrightLine FF01-525/39 (Semrock) were used. For measurements of H_2O_2 and ATP, SH-SY5Y cells were transiently transfected with the respective sensor using electroporation with the NEON transfection system (settings: 1100 V, 50 ms, 1 pulse; Thermo Fisher Scientific). HyPer, a genetically encoded sensor consisting of circularly permuted yellow fluorescent protein (cpYFP) inserted into the regulatory domain of the prokaryotic H_2O_2-sensing protein, OxyR (35) was used to measure cytosolic hydrogen peroxide. Excitation was set to 470 nm, same excitation and emission filters as for Oregon Green™ 488 BAPTA-1 were used. Ateam1.03, a FRET-based indicator for ATP composed of the ε subunit of the bacterial F_oF_1-ATP synthase sandwiched by CFP and YFP (33, 34) was used to measure cytosolic ATP levels. Excitation was set to 435 nm, excitation filter BrightLine FF01-434/17 (Semrock), and emission filter BrightLine FF01-470/28 (Semrock) were used. ATeam1.03-nD/nA/pcDNA3 was a gift from Takeharu Nagai (Addgene plasmid # 51958; http://n2t.net/addgene:51958; RRID:Addgene_51958). For ATP measurements, cells were subjected to media containing 10 mM 2-Deoxyglucose to inhibit glycolysis. The fluorescence lifetime was analyzed by the FLIMfit software tool developed at Imperial College London (89, 90).

ThT Assay

The aggregation of alpha-synuclein in-vitro was measured by Thioflavin T (ThT) assay. Briefly, 50 µL of 100 µM alpha-synuclein with 10 µM fresh ThT added, was incubated for 7 days with 1% DMSO as a control, 10 µM FCCP, 10 µM BAPTA-AM, or 10 µM BAPTA. Assays were performed in NUNC™ black 384-well plates with optical flat bottom (142761, Thermo Fisher Scientific) which were sealed with an Ampliseal transparent microplate sealer (Greiner Bio-One GmbH). Plates were incubated including orbital shaking at 300 rpm for 5 minutes before each read every hour at 37 °C for 170 cycles. The readings of ThT fluorescence intensity were taken using excitation at 440 nm and emission at 480 nm, collected from the bottom with 20 flashes per well and a gain setting of 1300 (FLUOstar Omega, BMG Labtec GmbH, Ortenberg, Germany). Experiments were repeated three times with four replicates for each condition.

Mitochondrial fragmentation

To label mitochondria, SH-SY5Y cells were incubated overnight with 1:1000 CellLight™ Mitochondria-RFP (Thermo Fisher Scientific) and imaged with a widefield microscope (as described in section cell culture). Images were taken randomly by automated imaging of a grid and images from 3 biological repeats were analyzed. The mitochondrial length was evaluated using the NIEL Mito algorithm (91, 92).

Animals

Adult female Sprague Dawley rats were supplied by Charles River UK Ltd., Scientific, Breeding and Supplying Establishment, registered under Animals (Scientific Procedures) Act 1986, and AAALAC International accredited. All animal work conformed to guidelines of animal husbandry as provided by the UK Home Office. Animals were sacrificed under schedule 1; procedures that do not require specific Home Office approval. Animal work was approved by the NACWO and University of Cambridge Ethics Board.

Mitochondrial isolation and Western blot analysis

Mitochondria were isolated from adult rat brain by differential centrifugation using mitochondria isolation kit for tissue (ab110168, abcam). Western blot for alpha-synuclein was performed using 4–12% Bis-Tris gels (Life Technologies), the protein was transferred onto 0.45 µm Millipore PVDF membrane (Fisher Scientific, Loughborough, UK) and subsequently fixed using 4% formaldehyde + 0.1% glutaraldehyde in PBS (both Sigma-Aldrich) (93). As primary antibody α-Synuclein (D37A6) XP® Rabbit mAb was used (1:1000 dilution, #4179, CST, Leiden, Netherlands). An enhanced chemiluminescence (ECL)-horse radish peroxidase (HRP) conjugated secondary antibody (NA934V, 1:1000 dilution, GE Healthcare, Uppsala, Sweden) and SuperSignal West Femto Chemiluminescent Substrate (Thermo Fisher Scientific) were used to probe the membrane, which was exposed using a G:BOX (Syngene, Cambridge, UK). Western blots were analyzed in FIJI (80).

TEM

SH-SY5Y cells and SH-SY5Y cells overexpressing YFP-alpha-synuclein were cultured in 6 well plates (Greiner Bio-One GmbH) at 350 000 per well. After reaching confluency cells were washed with 0.9% NaCl (Sigma-Aldrich) twice and incubated with 8% formaldehyde in 0.05 M sodium cacodylate buffer (Paraformaldehyde from Merck, Darmstadt, Germany) pH 7.4 for 2h at 4ºC. Cells were scraped from 6 wells and centrifuged for 10 min at 3500 g. Cells were washed 5 times in 0.05 M sodium cacodylate buffer, 3 times in deionized water, and incubated with 2 % uranyl acetate in 0.05 maleate buffer pH 5.2 (both BDH Chemicals Ltd., Dorset, UK) overnight at 4ºC. Cells were washed again and dehydrated at increasing ethanol concentrations (1x 50% EtOH, 3x 70% EtOH, 3x 95 % EtOH, 3x 100% EtOH, 3x 100 % dry EtOH; 5 min in each, Sigma-Aldrich). Cells were resuspended in LRW resin (LR White Resin, London Resin (Hard), Agar Scientific, Stansted, UK) mixed 50/50 with dry 100% EtOH and incubated overnight at room temperature. The following day, cells were spun down, and resuspended in pure LRW for 2 days, where LRW was exchanged twice. Cells were centrifuged at 13000 g to form a firm pellet, which was transferred to size 2 gelatine embedding capsules (TAAB, Aldermaston, UK) containing LRW resin. Gelatine capsules were covered with a glass coverslip to exclude any air and the resin was cured at 60ºC for 2 days. Gelatine capsules were removed and ultrathin sections were cut using a Leica Ultracut E Ultramicrotome (Leica, Wetzlar, Germany) and placed on 400 mesh nickel/formvar film grids (EM Resolutions). Sections were stained with Anti-GFP antibody (ab6556, Abcam) in blocking solution (2 % BSA (BBITM solutions, Crumlin, UK) in 10 mM TRIS (Sigma-Aldrich) buffer pH 7.4 containing 0.001% Triton-X100 (Calbiochem, San Diego, US) and 0.001% Tween20 (Sigma-Aldrich) at 1:100 overnight. After washing, sections were incubated with goat anti-rabbit 10 nm gold secondary antibody (BBITM solutions) in blocking solution at 1:200 for 1 hour. Sections were washed with washing buffer (same as above omitting BSA), deionized water and left for drying overnight. Post-staining included 2% uranyl acetate in 50 % methanol for 30 sec, followed by washing with 50 % methanol and 30-sec staining in Reynold's lead citrate (lead nitrate from BDH Biochemicals Ltd., Trisodiumcitrate from Sigma-Aldrich). Grids were rinsed thoroughly with deionized water and dried before imaging. Grids were imaged on an FEI Tecnai G2 electron microscope (Thermo Fisher Scientific) run at 200 keV using a 20 µm objective aperture, images were taken using an AMT V600 camera (AMT, Woburn, US).

In-vitro measurements of Aβ42 aggregation

Synthetic Aβ42 and Aβ42 Hilyte™ Fluor 488 (both from Anaspec, Seraing, Belgium) were prepared as previously described (94). Briefly, lyophilized Aβ42 (1 mg) was dissolved in ice-cold trifluroacetic acid (200 mL), sonicated at 0 °C for 60 s and then lyophilized overnight. Ice cold 1,1,1,3,3,3-hexafluro-2-propanol (1 mL) was added, sonicated at 0 °C for 60 s and aliquoted as 20 µL units. The samples were lyophilized overnight and were stored at -80 °C until use. Lyophilized Aβ42 Hilyte™ Fluor 488 peptide (0.1 mg) was dissolved in 1% NH_4OH (200 µL) and sonicated for 60 s at 0 °C. The sample was aliquoted into 5 µL units, snap-frozen in liquid nitrogen and stored at -80 °C. Immediately before the experiment unlabeled Aβ42 was prepared by adding first dimethyl sulfoxide (DMSO) (5% of total solvent volume), then sodium phosphate buffer (NaP buffer 50mM, pH 7.4) to reach a concentration of 20 µM. The solution was sonicated at 0 °C

for 3 min and centrifuged at 13,400 rpm at 0 °C for 30 min. Then the sample was further diluted to 5 µM concentration with NaP buffer. Also the labelled Aβ42 Hilyte™ Fluor 488 was brought to 5 µM concentration in NaP buffer and both were mixed in 1:1 ratio. Samples were prepared on ice adding Aβ42, 1 mg/mL of purified mitochondria (preparation see above) and 20 µM UCF-101. Mitochondria isolation buffer and DMSO were added in control samples. 12 µL volume were pipetted in silicon gaskets (Thermo Fisher Scientific, P24742) on a coverslip and measured at room temperature. Fluorescence lifetime measurements (FLIM) were carried out on a custom-built Time-Correlated Single Photon Counting (TCSPC) system as described above (see FLIM measurements of cytosolic calcium, H_2O_2, and ATP).

Statistics

Statistical analysis was performed using GraphPad Prism 6.07 (GraphPad Software, Inc., La Jolla, CA, USA). Values are given as mean ± SD unless otherwise stated. Normal distribution was tested using Shapiro-Wilk test. Two-tailed unpaired t-test was used upon normal distribution, two-tailed Mann-Whitney U test was used when no normal distribution was given. For multiple comparisons either one-way ANOVA with Dunnett's post hoc correction upon normal distribution or Kruskal-Wallis test with Dunn's multiple comparison when no normal distribution was given were performed. Significance was considered at $p < 0.05$.

Data availability.

All relevant data are available from the corresponding authors.

Acknowledgements

We would like to thank Karin H. Muller and Jeremy N. Skepper for their help and input for the transmission electron microscopy study. We would like to thank Samantha Beck for establishing the YFP-alpha-synuclein SH-SY5Y cell line.

Author contributions

J.L., A.F.V. and A.M. contributed to alpha-synuclein PFF assay and cell work. J.L performed FLIM experiments and mitochondrial morphology analysis. A.D.S. performed alpha-synuclein in-vitro work. J.L. and A.F.V. and C.H. contributed to Western blot analyses. J.L. performed TEM. J.L., S.W.V. and M.L. contributed to Aβ42 studies. J.M. and M.F. contributed to automated and SIM imaging. J.L. designed the experiments. J.L., C.F.K. and G.S.K.S. conducted the overall manuscript.

Funding

J.L. was supported by a research fellowship from the Deutsche Forschungsgemeinschaft (DFG; award LA 3609/2-1). G.S.K.S. and C.F.K. acknowledge funding from the Wellcome Trust, the UK Medical Research Council (MRC), Alzheimer Research UK (ARUK), and Infinitus China Ltd. C.F.K. acknowledges funding from the UK Engineering and Physical Sciences Research Council (EPSRC). J.L. and A.D.S. acknowledge Alzheimer Research UK (ARUK) travel grants.

Conflict of interest

The authors declare no conflict of interest.

References

1. de Lau, L. M. L., and Breteler, M. M. B. (2006) Epidemiology of Parkinson's disease. *Lancet Neurol*. **5**, 525–535

2. Polymeropoulos, M. H., Lavedan, C., Leroy, E., Ide, S. E., Dehejia, A., Dutra, A., Pike, B., Root, H., Rubenstein, J., Boyer, R., Stenroos, E. S., Chandrasekharappa, S., Athanassiadou, A., Papapetropoulos, T., Johnson, W. G., Lazzarini, A. M., Duvoisin, R. C., Iorio, G. Di, Golbe, L. I., and Nussbaum, R. L. (1997) Mutation in the α-Synuclein Gene Identified in Families with Parkinson ' s Disease. *Science.* **276**, 2045–2047

3. Spillantini, M. G., Schmidt, M. L., Lee, V. M., Trojanowski, J. Q., Jakes, R., and Goedert, M. (1997) Alpha-synuclein in Lewy bodies. *Nature*. **388**, 839–840

4. Chartier-Harlin, M., Kachergus, J., Roumier, C., Mouroux, V., Douay, X., and Lincoln, S. (2004) α-synuclein locus duplication as a cause of familial Parkinson's disease. *Lancet*. **364**, 1167–1169

5. Ibáñez, P., Bonnet, a-M., Débarges, B., Lohmann, E., Tison, F., Pollak, P., Agid, Y., Dürr, a, and Brice, a (2004) Causal relation between alpha-synuclein gene duplication and familial Parkinson's disease. *Lancet*. **364**, 1169–1171

6. Singleton, A. B., Farrer, M., Johnson, J., Singleton, A., Hague, S., and Kachergus, J. (2003) α-Synuclein Locus Triplication Causes Parkinson's Disease. *Science.* **302**, 841

7. Goate, A., Chartier-Harlin, M. C., Mullan, M., Brown, J., Crawford, F., Fidani, L., Giuffra, L., Haynes, A., Irving, N., and James, L. (1991) Segregation of a missense mutation in the amyloid precursor protein gene with familial Alzheimer's disease. *Nature*. **349**, 704–6

8. Murrell, J., Farlow, M., Ghetti, B., and D, B. M. (1991) A Mutation in the Amyloid Precursor Protein Associated with Hereditary Alzheimer's Disease. *Science.* **254**, 97–99

9. Citron, M., Westaway, D., Xia, W., Carlson, G., Diehl, T., Levesque, G., Johnson-Wood, K., Lee, M., Seubert, P., Davis, A., Kholodenko, D., Motter, R., Sherrington, R., Perry, B., Yao, H., Strome, R., Lieberburg, I., Rommens, J., Kim, S., Schenk, D., Fraser, P., St. George Hyslop, P., and Selkoe, D. J. (1997) Mutant presenilins of Alzheimer's disease increase production of 42-residue amyloid β-protein in both transfected cells and transgenic mice. *Nat. Med.* **3**, 67–72

10. Levy-Lahad, E., Wasco, W., Poorkaj, P., Romano, D. M., Oshima, J., Pettingell, W. H., Yu, C., Jondro, P. D., Schmidt, S. D., Wang, K., Crowley, A. C., Fu, Y., Guenette, S. Y., Galas, D., Nemens, E., Wijsman, E. M., Bird, T. D., Schellenberg, G. D., and Tanzi, R. E. (1995) Candidate Gene for the Chromosome 1 Familial Alzheimer 's Disease Locus. *Science.* **269**, 973–977

11. Sherrington, R., Rogaev, E. I., Liang, Y., Rogaeva, E. A., Levesque, G., Ikeda, M., Chi, H., Lin, C., Li, G., Holman, K., Tsuda, T., Mar, L., Foncin, J. F., Bruni, A. C., Montesi, M. P., Sorbi, S., Rainero, I., Pinessi, L., Nee, L., Chumakov, I., Pollen, D., Brookes, A., Sanseau, P., Polinsky, R. J., Wasco, W., Da Silva, H. A. R., Haines, J. L., Pericak-Vance, M. A., Tanzi, R. E., Roses, A. D., Fraser, P. E., Rommens, J. M., and St George-Hyslop, P. H. (1995) Cloning of a gene bearing missense mutations in early-onset familial Alzheimer's disease. *Nature.* **375**, 754–760

12. Langston, J., Ballard, P., Tetrud, J., and Irwin, I. (1983) Chronic Parkinsonism in humans due to a product of meperidine-analog synthesis. *Science.* **219**, 979–980

13. Burns, R. S., Chiueh, C. C., Markey, S. P., Ebert, M. H., Jacobowitz, D. M., and Kopin, I. J. (1983) A primate model of parkinsonism: selective destruction of dopaminergic neurons in the pars compacta of the substantia nigra by N-methyl-4-phenyl-1,2,3,6-tetrahydropyridine. *Proc. Natl. Acad. Sci.* **80**, 4546–4550

14. Betarbet, R., Sherer, T. B., Mackenzie, G., Garcia-Osuna, M., Panov, A. V, and Greenamyre, J. T. (2000) Chronic systemic pesticide exposure reproduces features of Parkinson's disease. *Nat.*

Neurosci. **3**, 1301–1306

15. Greenamyre, J. T., Sherer, T. B., Betarbet, R., and Panov, a V (2001) Complex I and Parkinson's disease. *IUBMB Life*. **52**, 135–141

16. Sherer, T. B., Kim, J.-H., Betarbet, R., and Greenamyre, J. T. (2003) Subcutaneous Rotenone Exposure Causes Highly Selective Dopaminergic Degeneration and α-Synuclein Aggregation. *Exp. Neurol.* **179**, 9–16

17. Valente, E. M., Abou-Sleiman, P. M., Caputo, V., Muqit, M. M. K., Harvey, K., Gispert, S., Ali, Z., Del Turco, D., Bentivoglio, A. R., Healy, D. G., Albanese, A., Nussbaum, R., González-Maldonado, R., Deller, T., Salvi, S., Cortelli, P., Gilks, W. P., Latchman, D. S., Harvey, R. J., Dallapiccola, B., Auburger, G., and Wood, N. W. (2004) Hereditary early-onset Parkinson's disease caused by mutations in PINK1. *Science.* **304**, 1158–1160

18. Todd, A. M., and Staveley, B. E. (2008) Pink1 suppresses α-synuclein-induced phenotypes in a Drosophila model of Parkinson's disease. *Genome*. **51**, 1040–1046

19. Todd, A. M., and Staveley, B. E. (2012) Expression of Pink1 with α-synuclein in the dopaminergic neurons of Drosophila leads to increases in both lifespan and healthspan. *Genet. Mol. Res.* **11**, 1497–1502

20. Oliveras-Salvá, M., Macchi, F., Coessens, V., Deleersnijder, A., Gérard, M., Van der Perren, A., Van den Haute, C., and Baekelandt, V. (2014) Alpha-synuclein-induced neurodegeneration is exacerbated in PINK1 knockout mice. *Neurobiol. Aging*. **35**, 2625–2636

21. Gispert, S., Brehm, N., Weil, J., Seidel, K., Rüb, U., Kern, B., Walter, M., Roeper, J., and Auburger, G. (2015) Potentiation of neurotoxicity in double-mutant mice with Pink1 ablation and A53T-SNCA overexpression. *Hum. Mol. Genet.* **24**, 1061–1076

22. Chung, S. Y., Kishinevsky, S., Mazzulli, J. R., Graziotto, J., Mrejeru, A., Mosharov, E. V., Puspita, L., Valiulahi, P., Sulzer, D., Milner, T. A., Taldone, T., Krainc, D., Studer, L., and Shim, J. won (2016) Parkin and PINK1 Patient iPSC-Derived Midbrain Dopamine Neurons Exhibit Mitochondrial Dysfunction and α-Synuclein Accumulation. *Stem Cell Reports*. **7**, 664–677

23. Creed, R. B., and Goldberg, M. S. (2019) Analysis of α-synuclein pathology in PINK1 knockout rat brains. *Front. Neurosci.* **13**, 1–6

24. Lautenschläger, J., Stephens, A. D., Fusco, G., Ströhl, F., Curry, N., Zacharopoulou, M., Michel, C. H., Laine, R., Nespovitaya, N., Fantham, M., Pinotsi, D., Zago, W., Fraser, P., Tandon, A., St George-Hyslop, P., Rees, E., Phillips, J. J., De Simone, A., Kaminski, C. F., and Schierle, G. S. K. (2018) C-terminal calcium binding of α-synuclein modulates synaptic vesicle interaction. *Nat. Commun.* **9**, 712

25. Luk, K. C., Song, C., O'Brien, P., Stieber, A., Branch, J. R., Brunden, K. R., Trojanowski, J. Q., and Lee, V. M.-Y. (2009) Exogenous alpha-synuclein fibrils seed the formation of Lewy body-like intracellular inclusions in cultured cells. *Proc. Natl. Acad. Sci. U. S. A.* **106**, 20051–6

26. Luk, K. C., Kehm, V. M., Zhang, B., O'Brien, P., Trojanowski, J. Q., and Lee, V. M. Y. (2012) Intracerebral inoculation of pathological α-synuclein initiates a rapidly progressive neurodegenerative α-synucleinopathy in mice. *J. Exp. Med.* **209**, 975–86

27. Peelaerts, W., Bousset, L., Van Der Perren, A., Moskalyuk, A., Pulizzi, R., Giugliano, M., Van Den Haute, C., Melki, R., and Baekelandt, V. (2015) α-Synuclein strains cause distinct synucleinopathies after local and systemic administration. *Nature.* **522**, 340–344

28. Pinotsi, D., Michel, C. H., Buell, A. K., Laine, R. F., Mahou, P., Dobson, C. M., Kaminski, C. F., and Kaminski, G. S. (2016) Nanoscopic insights into seeding mechanisms and toxicity of α -synuclein species in neurons. *PNAS.* **113**, 3815–3819

29. Thakur, P., Breger, L. S., Lundblad, M., Wan, O. W., Mattsson, B., Luk, K. C., Lee, V. M. Y., Trojanowski, J. Q., and Björklund, A. (2017) Modeling Parkinson's disease pathology by

combination of fibril seeds and α-synuclein overexpression in the rat brain. *Proc. Natl. Acad. Sci.* 10.1073/pnas.1710442114

30. Follett, J., Darlow, B., Wong, M. B., Goodwin, J., and Pountney, D. L. (2013) Potassium depolarization and raised calcium induces α-synuclein aggregates. *Neurotox. Res.* **23**, 378–92

31. Friedman, J. R., Lackner, L. L., West, M., DiBenedetto, J. R., Nunnari, J., and Voeltz, G. K. (2011) ER Tubules Mark Sites of Mitochondrial Division. *Science.* **334**, 358–362

32. Criddle, D. N., Gillies, S., Baumgartner-Wilson, H. K., Jaffar, M., Chinje, E. C., Passmore, S., Chvanov, M., Barrow, S., Gerasimenko, O. V., Tepikin, A. V., Sutton, R., and Petersen, O. H. (2006) Menadione-induced reactive oxygen species generation via redox cycling promotes apoptosis of murine pancreatic acinar cells. *J. Biol. Chem.* **281**, 40485–40492

33. Imamura, H., Nhat, K. P. H., Togawa, H., Saito, K., Iino, R., Kato-Yamada, Y., Nagai, T., and Noji, H. (2009) Visualization of ATP levels inside single living cells with fluorescence resonance energy transfer-based genetically encoded indicators. *Proc. Natl. Acad. Sci. U. S. A.* **106**, 15651–15656

34. Kotera, I., Iwasaki, T., Imamura, H., Noji, H., and Nagai, T. (2010) Reversible Dimerization of Aequorea victoria Fluorescent Proteins Increases the Dynamic Range of FRET-Based Indicators. *ACS Chem. Biol.* **5**, 321–332

35. Belousov, V. V, Fradkov, A. F., Lukyanov, K. A., Staroverov, D. B., Shakhbazov, K. S., Terskikh, A. V, and Lukyanov, S. (2006) Genetically encoded fluorescent indicator for intracellular hydrogen peroxide. *Nat. Methods*. **3**, 281–286

36. Bajar, B. T., Wang, E. S., Zhang, S., Lin, M. Z., and Chu, J. (2016) A guide to fluorescent protein FRET pairs. *Sensors (Switzerland)*. **16**, 1–24

37. Melo, E. P., Lopes, C., Gollwitzer, P., Lortz, S., Lenzen, S., Mehmeti, I., Kaminski, C. F., Ron, D., and Avezov, E. (2017) TriPer, an optical probe tuned to the endoplasmic reticulum tracks changes in luminal H2O2. *BMC Biol.* **15**, 1–15

38. Da Cruz, L. N., Alves, E., Leal, M. T., Juliano, M. A., Rosenthal, P. J., Juliano, L., and Garcia, C. R. S. (2011) FRET peptides reveal differential proteolytic activation in intraerythrocytic stages of the malaria parasites Plasmodium berghei and Plasmodium yoelii. *Int. J. Parasitol.* **41**, 363–372

39. Wang, L. F., Christensen, B. N., Bhatnagar, A., and Srivastava, S. K. (2001) Role of calcium-dependent protease(s) in globulization of isolated rat lens cortical fiber cells. *Investig. Ophthalmol. Vis. Sci.* **42**, 194–199

40. Ray, P., Chakrabarti, A. K., Broomfield, C. A., and Ray, R. (2002) Sulfur mustard-stimulated protease: A target for antivesicant drugs. *J. Appl. Toxicol.* **22**, 139–140

41. Demartino, G. N., Croall, D. E., and Calcium-dependent, D. E. (1982) Calcium-Dependent Proteases in Neuroblastoma Cells. *J. Neurochem.* **38**, 1642–1648

42. Mellgren, L. (1987) Calcium-dependent proteases: an enzyme system active at cellular membranes? *FASEB J.* **1**, 110–5

43. Gibellini, L., Pinti, M., Bartolomeo, R., De Biasi, S., Cormio, A., Musicco, C., Carnevale, G., Pecorini, S., Nasi, M., De Pol, A., and Cossarizza, A. (2015) Inhibition of Lon protease by triterpenoids alters mitochondria and is associated to cell death in human cancer cells. *Oncotarget*. **6**, 25466–83

44. Ruan, L., Zhou, C., Jin, E., Kucharavy, A., Zhang, Y., Wen, Z., Florens, L., and Li, R. (2017) Cytosolic proteostasis through importing of misfolded proteins into mitochondria. *Nature*. **543**, 443–446

45. Cilenti, L., Lee, Y., Hess, S., Srinivasula, S., Park, K. M., Junqueira, D., Davis, H., Bonventre, J. V., Alnemri, E. S., and Zervos, A. S. (2003) Characterization of a novel and specific inhibitor for the pro-apoptotic protease Omi/HtrA2. *J. Biol. Chem.* **278**, 11489–11494

46. Lu, M., Williamson, N., Mishra, A., Michel, C. H., Kaminski, C. F., Tunnacliffe, X. A., and Schierle, X. G. S. K. (2019) Structural progression of amyloid-beta Arctic mutant aggregation in cells revealed by multiparametric imaging. *J. Biol. Chem.* **294**, 1478–1487

47. Chen, W., Young, L. J., Lu, M., Zaccone, A., Strohl, F., Yu, N., Schierle, G. S. K., and Kaminski, C. F. (2017) Fluorescence self-quenching from reporter dyes informs on the structural properties of amyloid clusters formed in vitro and in cells. *Nano Lett.* **17**, 143–149

48. Kaminski Schierle, G. S., Bertoncini, C. W., Chan, F. T. S., Van Der Goot, A. T., Schwedler, S., Skepper, J., Schlachter, S., Van Ham, T., Esposito, A., Kumita, J. R., Nollen, E. A. A., Dobson, C. M., and Kaminski, C. F. (2011) A FRET sensor for non-invasive imaging of amyloid formation in vivo. *ChemPhysChem*. **12**, 673–680

49. Devi, L., Raghavendran, V., Prabhu, B. M., Avadhani, N. G., and Anandatheerthavarada, H. K. (2008) Mitochondrial import and accumulation of α-synuclein impair complex I in human dopaminergic neuronal cultures and Parkinson disease brain. *J. Biol. Chem.* **283**, 9089–9100

50. Cenini, G., Rub, C., Bruderek, M., and Voos, W. (2016) Amyloid β-peptides interfere with mitochondrial preprotein import competence by a coaggregation process. *Mol. Biol. Cell*. **27**, 3257–3272

51. Di Maio, R., Barrett, P. J., Hoffman, E. K., Barrett, C. W., Zharikov, A., Borah, A., Hu, X., McCoy, J., Chu, C. T., Burton, E. A., Hastings, T. G., and Greenamyre, J. T. (2016) α-synuclein binds to TOM20 and inhibits mitochondrial protein import in Parkinson's disease. *Sci. Transl. Med.* **8**, 1–14

52. Gurtubay, J. I. G., Goñi, F. M., Gómez-Fernández, J. C., Otamendi, J. J., and Macarulla, J. M. (1980) Triton X-100 solubilization of mitochondrial inner and outer membranes. *J. Bioenerg. Biomembr.* **12**, 47–70

53. Dabir, D. V., Hasson, S. A., Setoguchi, K., Johnson, M. E., Wongkongkathep, P., Douglas, C. J., Zimmerman, J., Damoiseaux, R., Teitell, M. A., and Koehler, C. M. (2013) A small molecule inhibitor of redox-regulated protein translocation into mitochondria. *Dev. Cell*. **25**, 81–92

54. Nunan, J., Shearman, M. S., Checler, F., Cappai, R., Evin, G., Beyreuther, K., Masters, C. L., and Small, D. H. (2001) The C-terminal fragment of the Alzheimer's disease amyloid protein precursor is degraded by a proteasome-dependent mechanism distinct from γ-secretase. *Eur. J. Biochem.* **268**, 5329–5336

55. Dehvari, N., Mahmud, T., Persson, J., Bengtsson, T., Graff, C., Winblad, B., Rönnbäck, A., and Behbahani, H. (2012) Amyloid precursor protein accumulates in aggresomes in response to proteasome inhibitor. *Neurochem. Int.* **60**, 533–542

56. Schmitz, A., Schneider, A., Kummer, M. P., and Herzog, V. (2004) Endoplasmic reticulum-localized amyloid β-peptide is degraded in the cytosol by two distinct degradation pathways. *Traffic*. **5**, 89–101

57. Strauss, K. M., Martins, L. M., Plun-Favreau, H., Marx, F. P., Kautzmann, S., Berg, D., Gasser, T., Wszolek, Z., Müller, T., Bornemann, A., Wolburg, H., Downward, J., Riess, O., Schulz, J. B., and Krüger, R. (2005) Loss of function mutations in the gene encoding Omi/HtrA2 in Parkinson's disease. *Hum. Mol. Genet.* **14**, 2099–2111

58. Bogaerts, V., Nuytemans, K., Reumers, J., Pals, P., Engelborghs, S., Pickut, B., Corsmit, E., Peeters, K., Schymkowitz, J., De Deyn, P. P., Cras, P., Rousseau, F., Theuns, J., and Van Broeckhoven, C. (2008) Genetic variability in the mitochondrial serine protease HTRA2 contributes to risk for Parkinson disease. *Hum. Mutat.* **29**, 832–840

59. Westerlund, M., Behbahani, H., Gellhaar, S., Forsell, C., Belin, A. C., Anvret, A., Zettergren, A., Nissbrandt, H., Lind, C., Sydow, O., Graff, C., Olson, L., Ankarcrona, M., and Galter, D. (2011) Altered enzymatic activity and allele frequency of OMI/HTRA2 in Alzheimer's disease. *FASEB J.* **25**, 1345–52

60. Unal Gulsuner, H., Gulsuner, S., Mercan, F. N., Onat, O. E., Walsh, T., Shahin, H., Lee, M. K., Dogu, O., Kansu, T., Topaloglu, H., Elibol, B., Akbostanci, C., King, M.-C., Ozcelik, T., and Tekinay, A. B. (2014) Mitochondrial serine protease HTRA2 p.G399S in a kindred with essential tremor and Parkinson disease. *Proc. Natl. Acad. Sci.* **111**, 18285–18290

61. Chao, Y. X., Ng, E. Y., Foo, J. N., Liu, J., Zhao, Y., and Tan, E. K. (2015) Mitochondrial serine protease HTRA2 gene mutation in Asians with coexistent essential tremor and Parkinson disease. *Neurogenetics*. **16**, 241–242

62. Jones, J. M., Datta, P., Srinivasula, S. M., Ji, W., Gupta, S., Zhang, Z. J., Davies, E., Hajnóczky, G., Saunders, T. L., Van Keuren, M. L., Fernandes-Alnemri, T., Meisler, M. H., and Alnemri, E. S. (2003) Loss of Omi mitochondrial protease activity causes the neuromuscular disorder of mnd2 mutant mice. *Nature*. **425**, 721–727

63. Martins, L. M., Morrison, A., Klupsch, K., Fedele, V., Moisoi, N., Teismann, P., Abuin, A., Grau, E., Geppert, M., George, P., Creasy, C. L., Martin, A., Hargreaves, I., Heales, S. J., Okada, H., Brandner, S., Schulz, B., Mak, T., Downward, J., and Livi, G. P. (2004) Neuroprotective Role of the Reaper-Related Serine Protease HtrA2 / Omi Revealed by Targeted Deletion in Mice. *Mol. Cell. Biol.* **24**, 9848–9862

64. Anandatheerthavarada, H. K., Biswas, G., Robin, M. A., and Avadhani, N. G. (2003) Mitochondrial targeting and a novel transmembrane arrest of Alzheimer's amyloid precursor protein impairs mitochondrial function in neuronal cells. *J. Cell Biol.* **161**, 41–54

65. Devi, L. (2006) Accumulation of Amyloid Precursor Protein in the Mitochondrial Import Channels of Human Alzheimer's Disease Brain Is Associated with Mitochondrial Dysfunction. *J. Neurosci.* **26**, 9057–9068

66. Mossmann, D., Vögtle, F. N., Taskin, A. A., Teixeira, P. F., Ring, J., Burkhart, J. M., Burger, N., Pinho, C. M., Tadic, J., Loreth, D., Graff, C., Metzger, F., Sickmann, A., Kretz, O., Wiedemann, N., Zahedi, R. P., Madeo, F., Glaser, E., and Meisinger, C. (2014) Amyloid-β peptide induces mitochondrial dysfunction by inhibition of preprotein maturation. *Cell Metab.* **20**, 662–669

67. Rui, Y., and Zheng, J. Q. (2016) Amyloid β oligomers elicit mitochondrial transport defects and fragmentation in a time-dependent and pathway-specific manner. *Mol. Brain*. **9**, 79

68. Subramaniam, S. R., Vergnes, L., Franich, N. R., Reue, K., and Chesselet, M. F. (2014) Region specific mitochondrial impairment in mice with widespread overexpression of alpha-synuclein. *Neurobiol. Dis.* **70**, 204–213

69. Lautenschäger, J., and Kaminski Schierle, G. S. (2019) Mitochondrial degradation of amyloidogenic proteins — A new perspective for neurodegenerative diseases. *Prog. Neurobiol.* **181**, 101660

70. Falkevall, A., Alikhani, N., Bhushan, S., Pavlov, P. F., Busch, K., Johnson, K. A., Eneqvist, T., Tjernberg, L., Ankarcrona, M., and Glaser, E. (2006) Degradation of the amyloid β-protein by the novel mitochondrial peptidasome, PreP. *J. Biol. Chem.* **281**, 29096–29104

71. Hansson Petersen, C. A., Alikhani, N., Behbahani, H., Wiehager, B., Pavlov, P. F., Alafuzoff, I., Leinonen, V., Ito, A., Winblad, B., Glaser, E., and Ankarcrona, M. (2008) The amyloid β-peptide is imported into mitochondria via the TOM import machinery and localized to mitochondrial cristae. *Proc. Natl. Acad. Sci. U. S. A.* **105**, 13145–50

72. Fang, D., Wang, Y., Zhang, Z., Du, H., Yan, S., Sun, Q., Zhong, C., Wu, L., Vangavaragu, J. R., Yan, S., Hu, G., Guo, L., Rabinowitz, M., Glaser, E., Arancio, O., Sosunov, A. A., McKhann, G. M., Chen, J. X., and Yan, S. S. Du (2015) Increased neuronal PreP activity reduces Aβ accumulation, attenuates neuroinflammation and improves mitochondrial and synaptic function in Alzheimer disease's mouse model. *Hum. Mol. Genet.* **24**, 5198–5210

73. Sherer, T. B., Betarbet, R., Testa, C. M., Seo, B. B., Richardson, J. R., Kim, J. H., Miller, G. W., Yagi, T., Matsuno-Yagi, A., and Greenamyre, J. T. (2003) Mechanism of toxicity in

rotenone models of Parkinson's disease. *J Neurosci*. **23**, 10756–10764

74. Guzman, J. N., Ilijic, E., Yang, B., Sanchez-Padilla, J., Wokosin, D., Galtieri, D., Kondapalli, J., Schumacker, P. T., and Surmeier, D. J. (2018) Systemic isradipine treatment diminishes calcium-dependent mitochondrial oxidant stress. *J. Clin. Invest.* 10.1172/JCI95898

75. Dull, T., Zufferey, R., Kelly, M., Mandel, R. J., Nguyen, M., Trono, D., and Naldini, L. (1998) A third-generation lentivirus vector with a conditional packaging system. *J. Virol.* **72**, 8463–71

76. Sancak, Y., Peterson, T. R., Shaul, Y. D., Lindquist, R. A., Thoreen, C. C., Bar-Peled, L., and Sabatini, D. M. (2008) The rag GTPases bind raptor and mediate amino acid signaling to mTORC1. *Science.* **320**, 1496–1501

77. Wu, H., Zhang, F., Williamson, N., Jian, J., Zhang, L., Liang, Z., Wang, J., An, L., Tunnacliffe, A., and Zheng, Y. (2014) Effects of secondary metabolite extract from Phomopsis occultaon β-amyloid aggregation. *PLoS One.* 10.1371/journal.pone.0109438

78. Plun-Favreau, H., Klupsch, K., Moisoi, N., Gandhi, S., Kjaer, S., Frith, D., Harvey, K., Deas, E., Harvey, R. J., McDonald, N., Wood, N. W., Martins, L. M., and Downward, J. (2007) The mitochondrial protease HtrA2 is regulated by Parkinson's disease-associated kinase PINK1. *Nat. Cell Biol.* **9**, 1243–1252

79. Edelstein, A. D., Tsuchida, M. A., Amodaj, N., Pinkard, H., Vale, R. D., and Stuurman, N. (2014) Advanced methods of microscope control using μManager software. *J. Biol. Methods*. **1**, 10

80. Schindelin, J., Arganda-Carreras, I., Frise, E., Kaynig, V., Longair, M., Pietzsch, T., Preibisch, S., Rueden, C., Saalfeld, S., Schmid, B., Tinevez, J.-Y., White, D. J., Hartenstein, V., Eliceiri, K., Tomancak, P., and Cardona, A. (2012) Fiji: an open-source platform for biological-image analysis. *Nat. Methods*. **9**, 676–682

81. de Chaumont, F., Dallongeville, S., Chenouard, N., Hervé, N., Pop, S., Provoost, T., Meas-Yedid, V., Pankajakshan, P., Lecomte, T., Le Montagner, Y., Lagache, T., Dufour, A., and Olivo-Marin, J.-C. (2012) Icy: an open bioimage informatics platform for extended reproducible research. *Nat. Methods*. **9**, 690–696

82. Arai, K., and Barakbah, A. R. (2007) Hierarchical K-means: an algorithm for centroids initialization for K-means. *Rep. Fac. Sci. Engrg.* **36**, 36–125

83. Huang, C., Ren, G., Zhou, H., and Wang, C. (2005) A new method for purification of recombinant human alpha-synuclein in Escherichia coli. *Protein Expr. Purif.* **42**, 173–177

84. Campioni, S., Carret, G., Jordens, S., Ce Nicoud, L., Mezzenga, R., and Riek, R. (2014) The Presence of an Air−Water Interface Affects Formation and Elongation of α‑Synuclein Fibrils. JACS 10.1021/ja412105t

85. Marchenko, S., and Flanagan, L. (2007) Immunocytochemistry: human neural stem cells. *J. Vis. Exp.* 10.3791/267

86. Young, L. J., Ströhl, F., and Kaminski, C. F. (2016) A Guide to Structured Illumination TIRF Microscopy at High Speed with Multiple Colors. *J. Vis. Exp.* 10.3791/53988

87. Müller, M., Mönkemöller, V., Hennig, S., Hübner, W., and Huser, T. (2016) Open-source image reconstruction of super-resolution structured illumination microscopy data in ImageJ. *Nat. Commun.* **7**, 1–6

88. Chen, W. Y., Avezov, E., Schlachter, S. C., Gielen, F., Laine, R. F., Harding, H. P., Hollfelder, F., Ron, D., and Kaminski, C. F. (2015) A method to quantify FRET stoichiometry with phasor plot analysis and acceptor lifetime ingrowth. *Biophys. J.* **108**, 999–1002

89. Görlitz, F., Kelly, D. J., Warren, S. C., Alibhai, D., West, L., Kumar, S., Alexandrov, Y., Munro, I., Garcia, E., McGinty, J., Talbot, C., Serwa, R. A., Thinon, E., da Paola, V., Murray, E. J., Stuhmeier, F., Neil, M. A. A., Tate, E. W., Dunsby, C., and French, P. M. W. (2017) Open Source High Content Analysis Utilizing Automated Fluorescence Lifetime Imaging

Microscopy. *J. Vis. Exp.* 10.3791/55119

90. Warren, S. C., Margineanu, A., Alibhai, D., Kelly, D. J., Talbot, C., Alexandrov, Y., Munro, I., Katan, M., Dunsby, C., and French, P. M. W. (2013) Rapid Global Fitting of Large Fluorescence Lifetime Imaging Microscopy Datasets. *PLoS One*. 10.1371/journal.pone.0070687

91. Lautenschläger, J., Lautenschläger, C., Tadic, V., Suesse, H., Ortmann, W., Denzler, J., Stallmach, A., Witte, O. W., and Grosskreutz, J. (2015) Novel computer vision algorithm for the reliable analysis of organelle morphology in whole cell 3D images - A pilot study for the quantitative evaluation of mitochondrial fragmentation in amyotrophic lateral sclerosis. *Mitochondrion*. **25**, 49–59

92. Herbert, S., Ortmann, W., Lautenschl, J., Marco, K., Grosskreutz, J., and Denzler, J. (2014) Quantitative Analysis of Pathological Mitochondrial Morphology in Neuronal Cells in Confocal Laser Scanning Microscopy Images. *Proc. IWBBIO*

93. Lee, B. R., and Kamitani, T. (2011) Improved immunodetection of endogenous α-synuclein. *PLoS One*. **6**, e23939

94. Sum, T. H., Sum, T. J., Galloway, W. R. J. D., Collins, S., Twigg, D. G., Hollfelder, F., and Spring, D. R. (2016) Combinatorial synthesis of structurally diverse triazole-bridged flavonoid dimers and trimers. *Molecules*. 10.3390/molecules21091230

Figure Legends

Fig. 1. BAPTA-AM treatment increases alpha-synuclein pathology.
(A) YFP-alpha-synuclein SH-SY5Y cells were treated with DMSO (control), 10 µM BAPTA-AM for 1h (before fibrillar seed incubation) and for 5h (before plus during the incubation with alpha-synuclein fibrillar seeds). Scale bars: 20 µm. Alpha-synuclein seeding was increased upon 1h pre-treatment and 5h treatment with BAPTA-AM. Data are presented as mean ± SD. *p = 0.0127 and ****p < 0.0001 (Kruskal-Wallis test with Dunn's multiple comparison). N = 16, 9, 15 with n = regions analyzed, three biological repeats.
(B) Fluorescence lifetime images of cytosolic calcium levels (Oregon Green™ 488 BAPTA-1 fluorescence lifetime) in SH-SY5Y cells treated with DMSO (control), 10 µM BAPTA-AM for 10 min, 1h or 5h. Scale bars: 20 µm. The cytosolic calcium level within cells was significantly reduced upon 10 min incubation with BAPTA-AM, however after 1h of incubation with BAPTA-AM calcium levels returned back to basal levels. After 5h treatment with BAPTA-AM calcium levels significantly increased beyond basal calcium levels. Data are presented as mean ± SD. ****p < 0.0001 (Kruskal-Wallis test with Dunn's multiple comparison). N = 88, 54, 61, 46, with n = cells analyzed, three biological repeats.
(C) ThT assay displaying the aggregation kinetics of alpha-synuclein in-vitro in the presence of DMSO, 10 µM BAPTA-AM, or 10 µM BAPTA. Data are presented from three biological repeats.
(D) Mito-RFP stained mitochondrial network in SH-SH5Y cells. Cells were treated with DMSO (control) or 10 µM BAPTA-AM for 5h. Scale bars: 5 µm.
(E) YFP-alpha-synuclein overexpressing SH-SY5Y cells treated with DMSO (control), 10 µM FCCP for 1h (before fibrillar seed incubation) and for 5h (before plus during the incubation with alpha-synuclein fibrillar seeds). Scale bars: 20 µm. Alpha-synuclein aggregation was increased upon 5h treatment with FCCP. Data are presented as mean ± SD. *p = 0.0374 (Kruskal-Wallis test with Dunn's multiple comparison). N = 9, 6, 8 with n = regions analyzed, three biological repeats.
(F) ThT assay displaying the aggregation kinetics of alpha-synuclein in-vitro in the presence of DMSO or 10 µM FCCP. Data are presented from three biological repeats.

Fig. 2. Downstream effectors of mitochondrial dysfunction do not influence alpha-synuclein pathology.
(A) YFP-alpha-synuclein SH-SY5Y cells were treated with DMSO (control), 500 µM MPP^+, 1 µM ionomycin, or 3 µM menadione for 3 days (1h before, during alpha-synuclein fibrillar seed incubation, and during the 3 day period until evaluation). Scale bars: 20 µm. Alpha-synuclein seeding was not significantly increased (one-way ANOVA with Dunnett's post-hoc correction). Data are presented as mean ± SD, N = 11, 8, 8, 7 with n = regions analyzed, three biological repeats.
(B) Fluorescence lifetime images and graphs for ATP levels (Ateam1.03 donor fluorescence lifetime) in SH-SY5Y cells treated with DMSO (control), 500 µM MPP^+, 10 µM FCCP and 10 µM BAPTA-AM for 1h. MPP^+ and FCCP significantly decreased ATP levels, BAPTA-AM had no significant effect. ****p < 0.0001 and N = 43, 74, 48, 47.
(C) Fluorescence lifetime images and graphs for cytosolic calcium levels (Oregon Green™ 488 BAPTA-1 fluorescence lifetime) in SH-SY5Y cells treated with DMSO (control), 1 µM ionomycin, 10 µM FCCP and 10 µM BAPTA-AM for 1h. Ionomycin and FCCP significantly increased cytosolic calcium levels. ****p < 0.0001 and N = 88, 60, 42, 61.
(D) Fluorescence lifetime images and graphs of H_2O_2 levels (HyPer fluorescence lifetime) in SH-SY5Y cells treated with DMSO (control), 3 µM menadione, 10 µM FCCP and 10 µM BAPTA-AM for 1h. Menadione, FCCP and BAPTA-AM significantly increased H_2O_2 levels. Both, FCCP and BAPTA-AM did not produce higher H_2O_2 levels than seen with menadione. **p = 0.0017, p = 0.0012 and p = 0.0058 and N = 79, 63, 36, 70. All scale bars: 20 µm. All data are presented as mean ± SD with n = cells analyzed, Kruskal-Wallis test with Dunn's multiple comparison, three biological repeats.

Fig. 3. Inhibition of mitochondrial proteases increases alpha-synuclein pathology.
(A and B) Quantification of mitochondrial fragmentation after 5h treatment with 10 µM FCCP, 10 µM BAPTA-AM, 500 µM MPP^+, 1 µM ionomycin and 3 µM menadione. The mitochondrial length was significantly decreased after treatment with FCCP and BAPTA-AM. Scale bars: 10 µm. Data are

presented as mean ± SD. ****p < 0.0001 (Kruskal-Wallis test with Dunn's multiple comparison). N = 76, 92, 103, 90, 88, 89 with n = individual images, three biological repeats. Image analysis of mitochondrial fragmentation was performed using NIEL Mito (91).
(C) YFP-alpha-synuclein SH-SY5Y cells were treated with DMSO (control), 1 µM CDDO-Me, or 20 µM UCF-101 before and during the incubation with alpha-synuclein fibrillar seeds (5h). Scale bars: 20 µm. Alpha-synuclein aggregation was increased upon both treatments. Data are presented as mean ± SD. **p = 0.005 and ****p < 0.0001 (Kruskal-Wallis test with Dunn's multiple comparison). N = 15, 9, 11 with n = regions analyzed, three biological repeats.

Fig. 4. Mitochondrial proteostasis influences Amyloid β 1-42 pathology.
(A) Aβ42-mCherry overexpressing HEK cells were treated with DMSO (control), 1 µM FCCP or 10 µM BAPTA-AM for 24 h. The aggregation of Aβ42 was increased upon treatment with FCCP and BAPTA-AM. Data are presented as mean ± SD. *p = 0.0298 and ****p < 0.0001 (Kruskal-Wallis test with Dunn's multiple comparison). N = 9 for all conditions, with n = wells analyzed, three biological repeats.
(B) Aβ42-mCherry cells were treated with DMSO (control), 0.1 µM CDDO-Me or 20 µM UCF-101 for 24 h. The aggregation of Aβ42 was increased upon treatment with UCF-101. Data are presented as mean ± SD. ***p = 0.0001 (one-way ANOVA with Dunnett's post-hoc correction). N = 9 for all conditions, with n = wells analyzed, three biological repeats.
(C) Aβ42-mCherry cells were transfected with either uncut pcDNA3 (control) or HtrA2 pcDNA3 and Aβ42-mCherry expression was induced with tetracycline for 3 days. The aggregation of Aβ42 was significantly decreased upon overexpression of HtrA2. Data are presented as mean ± SD. **p = 0.0089 (two-tailed unpaired t-test). N = 36, 34 with n = images analyzed, four biological repeats. Scale bars: 20 µm.

Fig. 5. HtrA2 influences in-vitro aggregation of Aβ42.
(A) Fluorescence lifetime images of Hilyte™ Fluor 488 labelled Aβ42 at the beginning of the experiment (t0) and after 2 h of incubation at room temperature (t2h) show a decrease in fluorescence lifetime in control conditions demonstrating protein aggregation. No decrease in Aβ42 Hilyte™ Fluor 488 fluorescence lifetime was seen when isolated mitochondria were present. Data are presented as mean ± SD. **p = 0.0025 and ****p < 0.0001 (one-way ANOVA with Tukey's post-hoc correction). N = 7, 8, 7, 7 with n = wells analyzed, three biological repeats. Scale bars: 20 µm.
(B) Fluorescence lifetime images of Hilyte™ Fluor 488 labelled Aβ42 at the beginning of the experiment (t0) and after 2 h of incubation at room temperature (t2h), showing a decrease in the Aβ42 Hilyte™ Fluor 488 fluorescence lifetime when UCF-101 treated mitochondria were present. Data are presented as mean ± SD. ***p =0.0009 and *p= 0.0142 (one-way ANOVA with Tukey's post-hoc correction). N = 8, 8, 7, 8 with n = wells analyzed, three biological repeats. Scale bars: 20 µm.

Fig. 6. Inhibition of mitochondrial protein import increases alpha-synuclein and Aβ42 pathology.
(A) Transmission electron microscopy (TEM) image of immunogold labelled YFP-alpha-synuclein in SH-SY5Y cells showing that alpha-synuclein is contained within mitochondria. Arrows indicate individual immunogold labels within mitochondria. m = mitochondria, cyt = cytoplasm. Scale bar: 100 nm.
(B) Alpha-synuclein of isolated mitochondria from adult rat brain in the absence (native) of proteinase K (PK), in the presence of PK, or in the presence of both PK and 0.1% TritonX-100.
(C) Relative intensity of alpha-synuclein bands normalized to native mitochondria. Data are presented as mean ± SD. ***p = 0.0007, ****p = < 0.0001, **p = 0.0017 (one-way ANOVA with Tukey's post-hoc correction). N = 3 for all conditions with n = biological repeats.
(D) YFP-alpha-synuclein SH-SY5Y were cells treated with DMSO (control), or 50 µM MitobloCK-6 before and during the incubation with alpha-synuclein fibrillar seeds (5h). Scale bars: 20 µm. Alpha-synuclein seeding was significantly increased upon treatment. Data are presented as mean ± SD. ****p < 0.0001 (two-tailed Mann-Whitney U test). N = 15, 11 with n = regions analyzed, three biological repeats.
(E) Aβ42-mCherry cells were treated with DMSO (control) or 5 µM MitobloCK-6 for 24 h. Scale bars: 20 µm. The aggregation of Aβ42 was increased upon treatment with MitobloCK-6. Data are presented

as mean ± SD. **p = 0.0088 (two-tailed unpaired t-test). N = 9 for all conditions, with n = wells analyzed, three biological repeats.
(F) Aβ42-mCherry cells were treated with DMSO (control), 10 nM bafilomycin A1, 0.5 μM MG132 or 50 nM 17-AAG for 24 h. Scale bars: 20 μm. The aggregation of Aβ42 was significantly increased upon treatment with MG132. Data are presented as mean ± SD. ****p < 0.0001 (Kruskal-Wallis test with Dunn's multiple comparison). N = 23, 24, 24, 24 with n = images analyzed, three biological repeats.

Figures

Figure 1

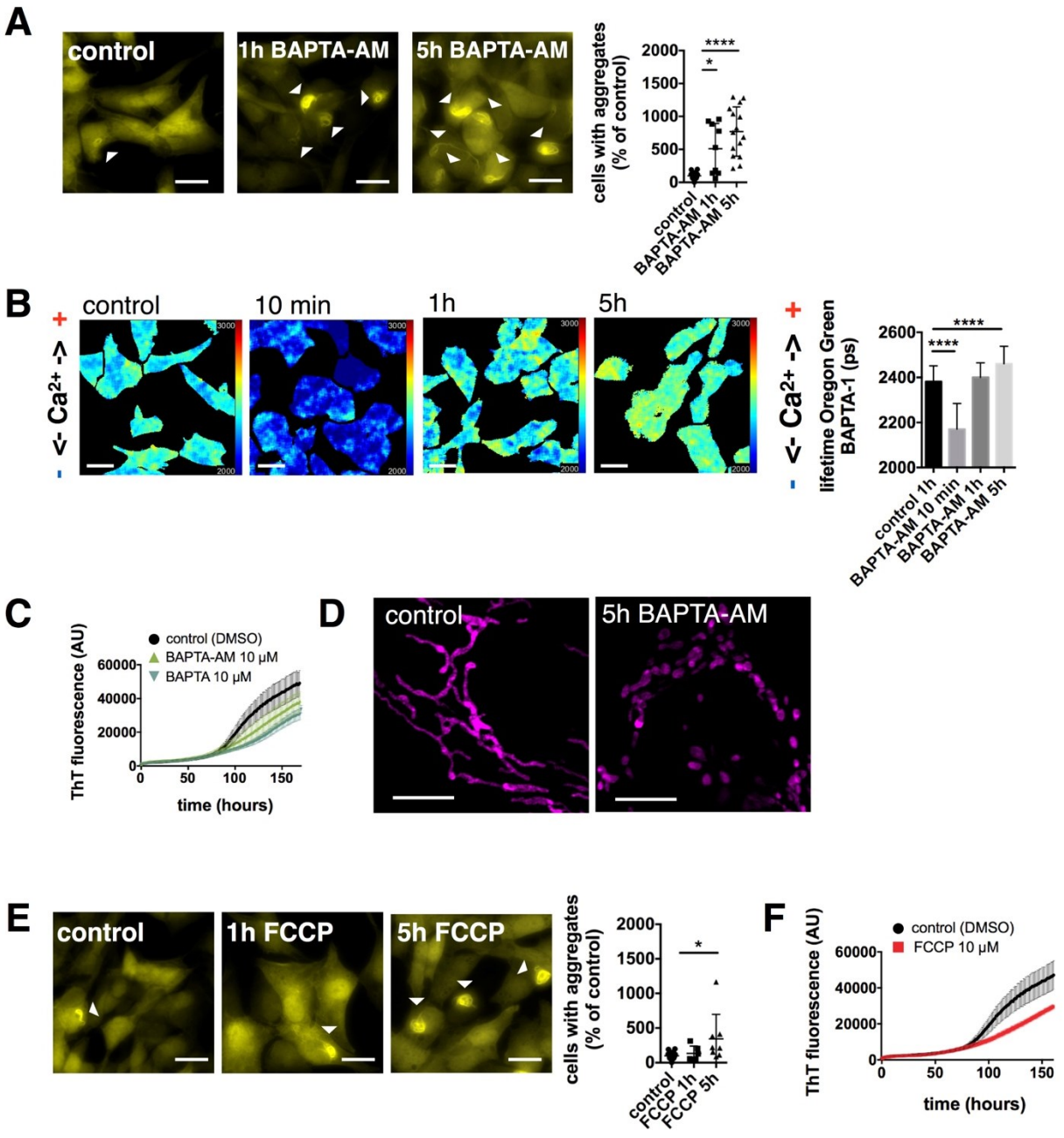

Figure 2

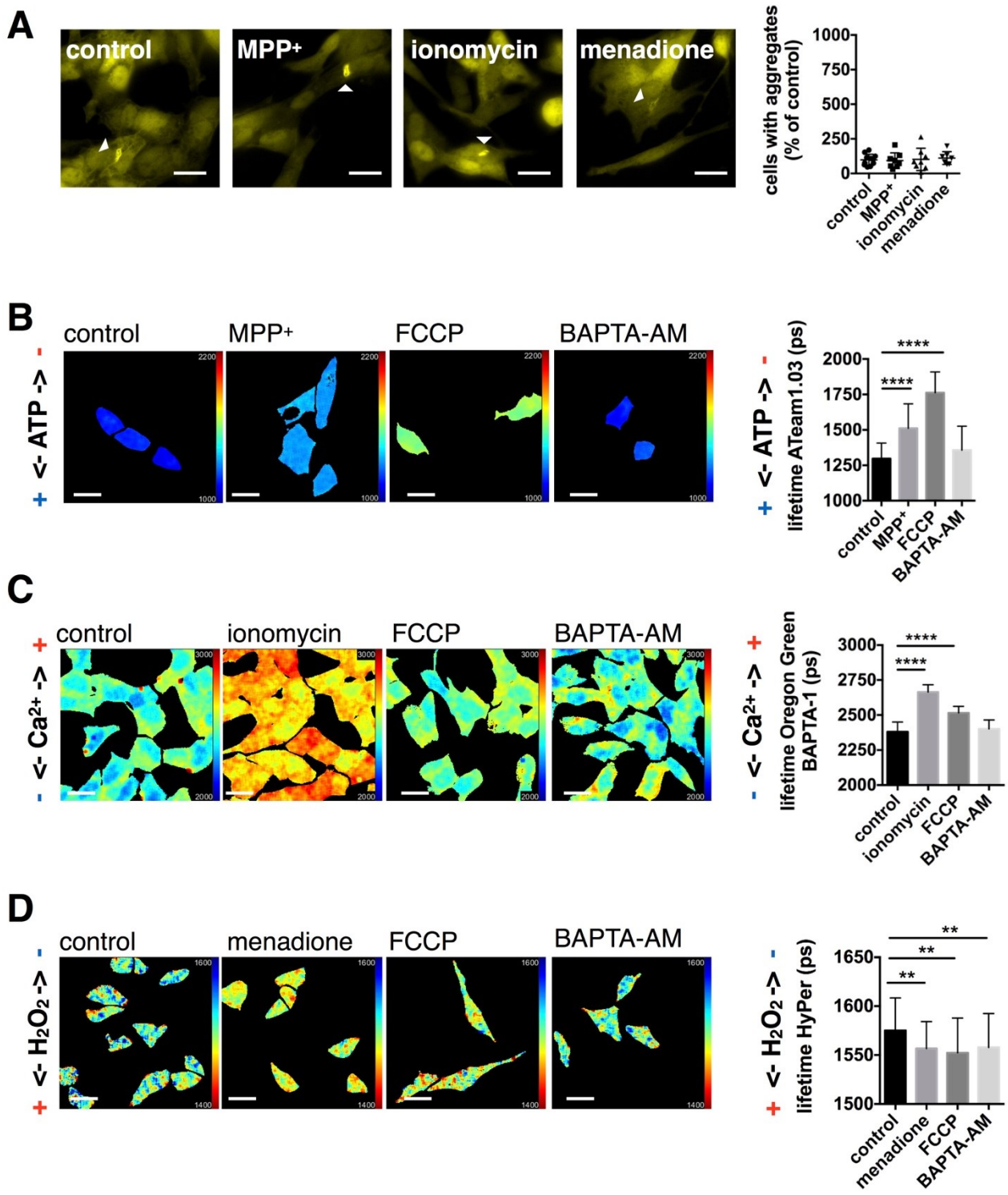
A
control
MPP+
ionomycin
menadione
cells with aggregates (% of control)
1000
750
500
250
0
control
MPP+
ionomycin
menadione
B
control
MPP+
FCCP
BAPTA-AM
<- ATP ->
+
-
2200
1000
lifetime ATeam1.03 (ps)
2000
1750
1500
1250
1000
****
****
control
MPP+
FCCP
BAPTA-AM
C
control
ionomycin
FCCP
BAPTA-AM
<- Ca2+ ->
3000
2000
lifetime Oregon Green BAPTA-1 (ps)
3000
2750
2500
2250
2000
****
****
control
ionomycin
FCCP
BAPTA-AM
D
control
menadione
FCCP
BAPTA-AM
<- H2O2 ->
1600
1400
lifetime HyPer (ps)
1650
1600
1550
1500
**
**
**
control
menadione
FCCP
BAPTA-AM

Figure 3

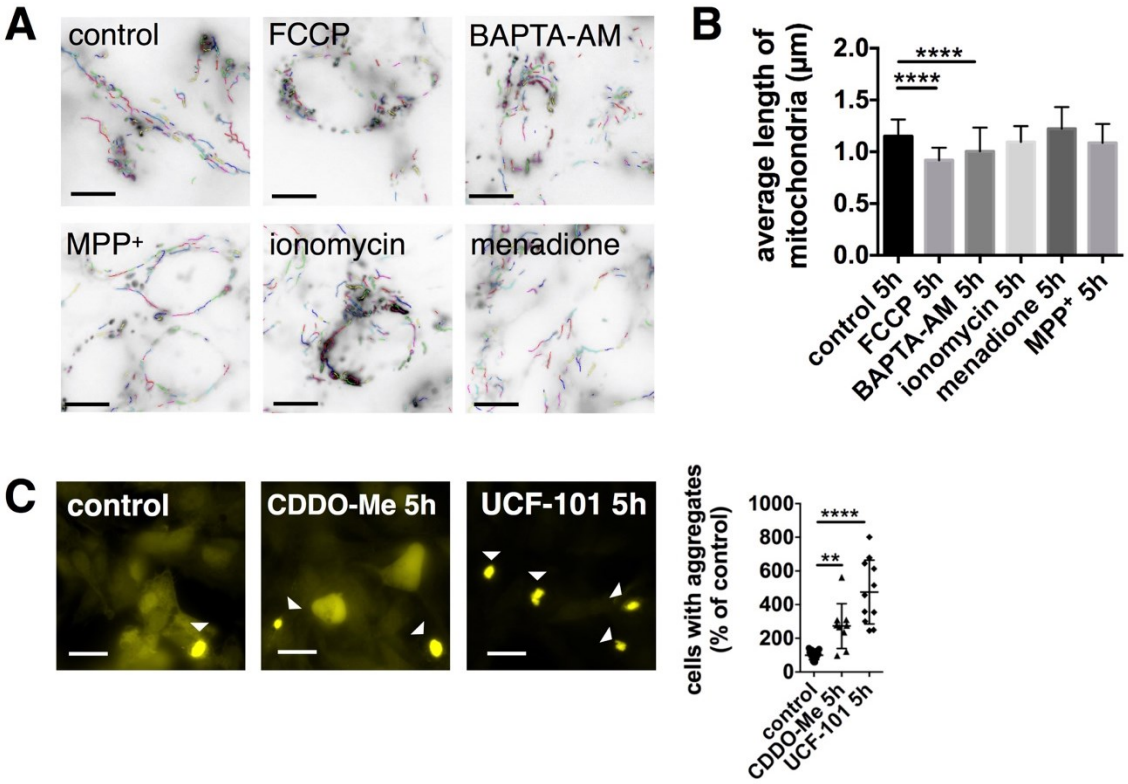
A
control
FCCP
BAPTA-AM
MPP+
ionomycin
menadione
B
average length of mitochondria (µm)
2.0
1.5
1.0
0.5
0.0
****
****
control 5h
FCCP 5h
BAPTA-AM 5h
ionomycin 5h
menadione 5h
MPP+ 5h
C
control
CDDO-Me 5h
UCF-101 5h
cells with aggregates (% of control)
1000
800
600
400
200
0
****
**
control
CDDO-Me 5h
UCF-101 5h

Figure 4

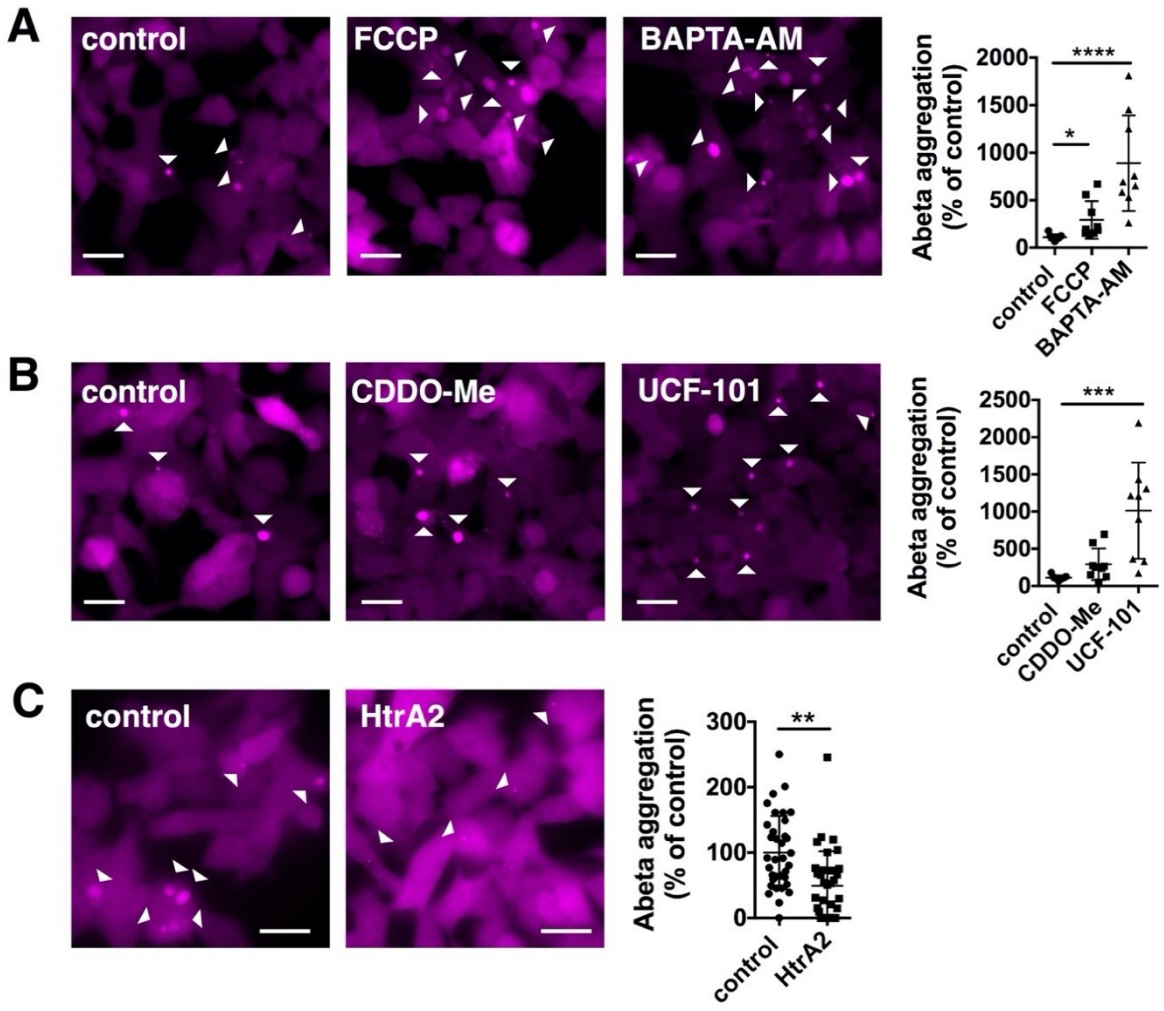
A
control
FCCP
BAPTA-AM
Abeta aggregation (% of control)
2000
1500
1000
500
0
****
*
control
FCCP
BAPTA-AM
B
control
CDDO-Me
UCF-101
Abeta aggregation (% of control)
2500
2000
1500
1000
500
0
***
control
CDDO-Me
UCF-101
C
control
HtrA2
Abeta aggregation (% of control)
300
200
100
0
**
control
HtrA2

Figure 5

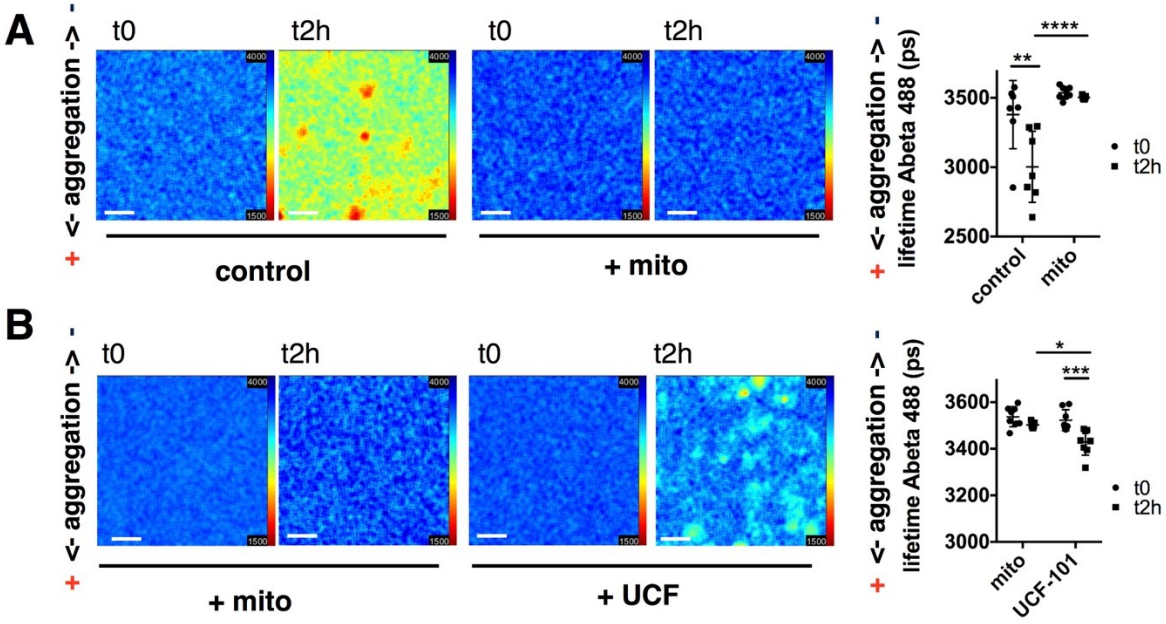
A
t0
t2h
t0
t2h
- <- aggregation -> +
control
+ mito
lifetime Abeta 488 (ps)
**
****
3500
3000
2500
control
mito
t0
t2h
B
t0
t2h
t0
t2h
+ mito
+ UCF
*
***
3600
3400
3200
3000
mito
UCF-101

Figure 6

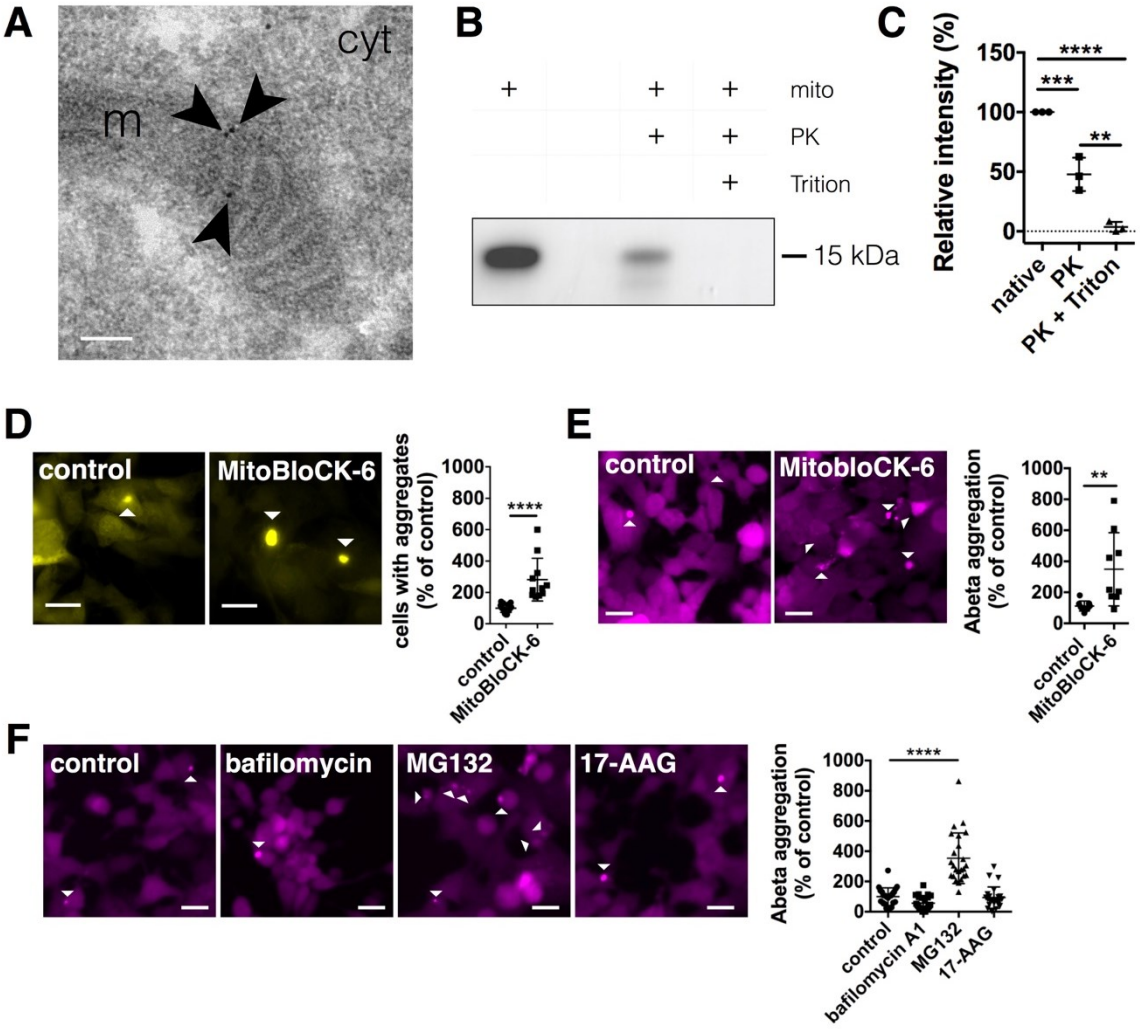
A
cyt
m
B
+
+
+
mito
+
+
PK
+
Trition
15 kDa
C
Relative intensity (%)
150
100
50
0
****
***
**
native
PK
PK + Triton
D
control
MitoBloCK-6
cells with aggregates (% of control)
1000
800
600
400
200
0
****
control
MitoBloCK-6
E
control
MitobloCK-6
Abeta aggregation (% of control)
1000
800
600
400
200
0
**
control
MitoBloCK-6
F
control
bafilomycin
MG132
17-AAG
Abeta aggregation (% of control)
1000
800
600
400
200
0
****
control
bafilomycin A1
MG132
17-AAG

Supplementary Figure 1

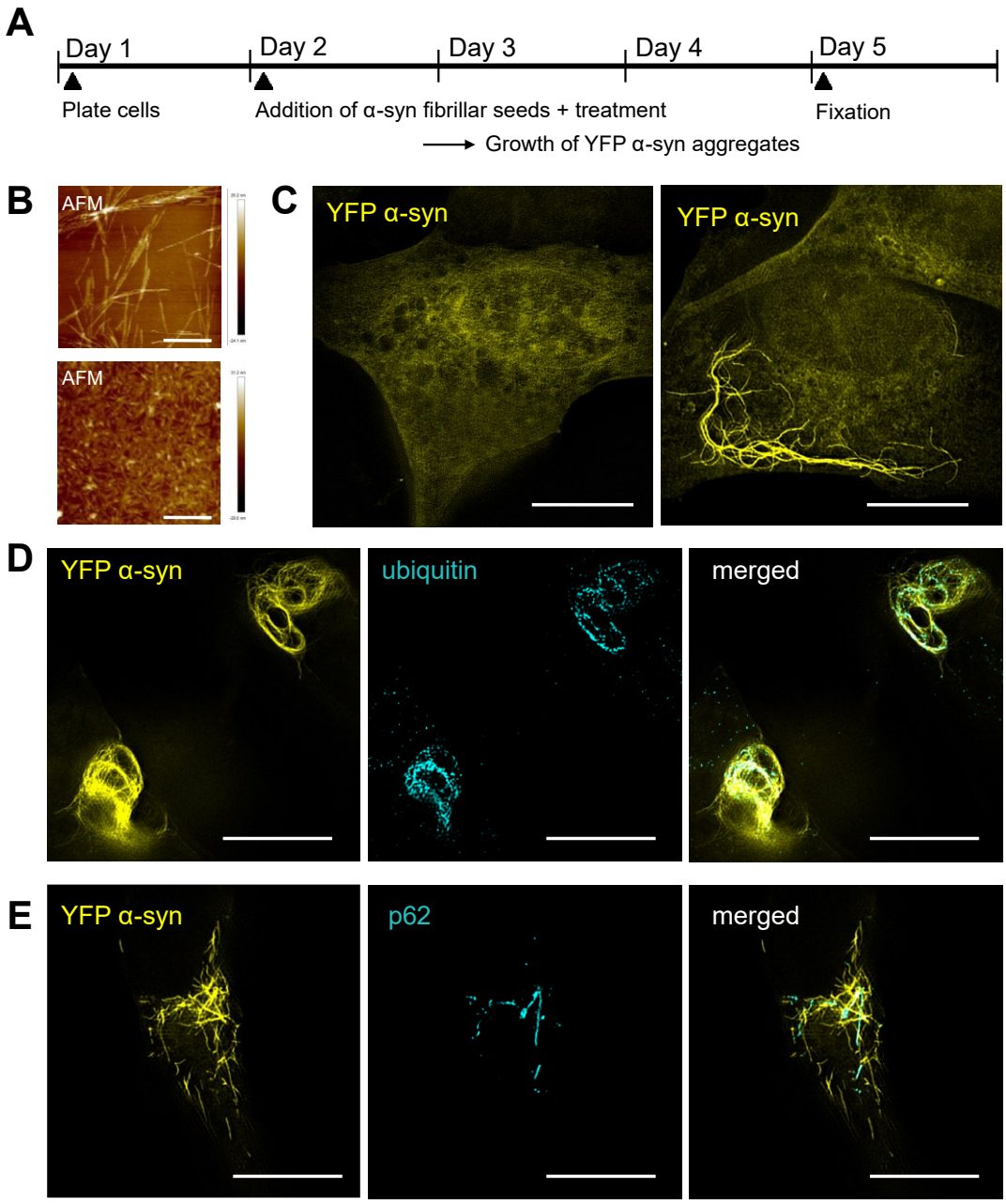

Supplementary Fig. 1. Incubation of SH-SY5Y cells overexpressing YFP-alpha-synuclein with alpha-synuclein seeds leads to YFP-alpha-synuclein fibril formation.
(A) Schematic overview of the cellular alpha-synuclein aggregation/seeding assay.
(B) Fibrillar seeds generated from recombinant human wild-type alpha-synuclein shown by atomic force microscopy before (upper panel) and after sonication (lower panel). Scale bars: 1 µm.
(C) Structured illumination microscopy (SIM) images of SH-SY5Y cells overexpressing YFP-tagged alpha-synuclein in the absence (left) and upon incubation with alpha-synuclein fibrillar seeds (right). Scale bars: 10 µm.
(D and E) Co-staining of YFP-alpha-synuclein fibrillar aggregates with ubiquitin and ubiquitin-binding protein p62. Scale bars: 10 µm.

Supplementary Figure 2

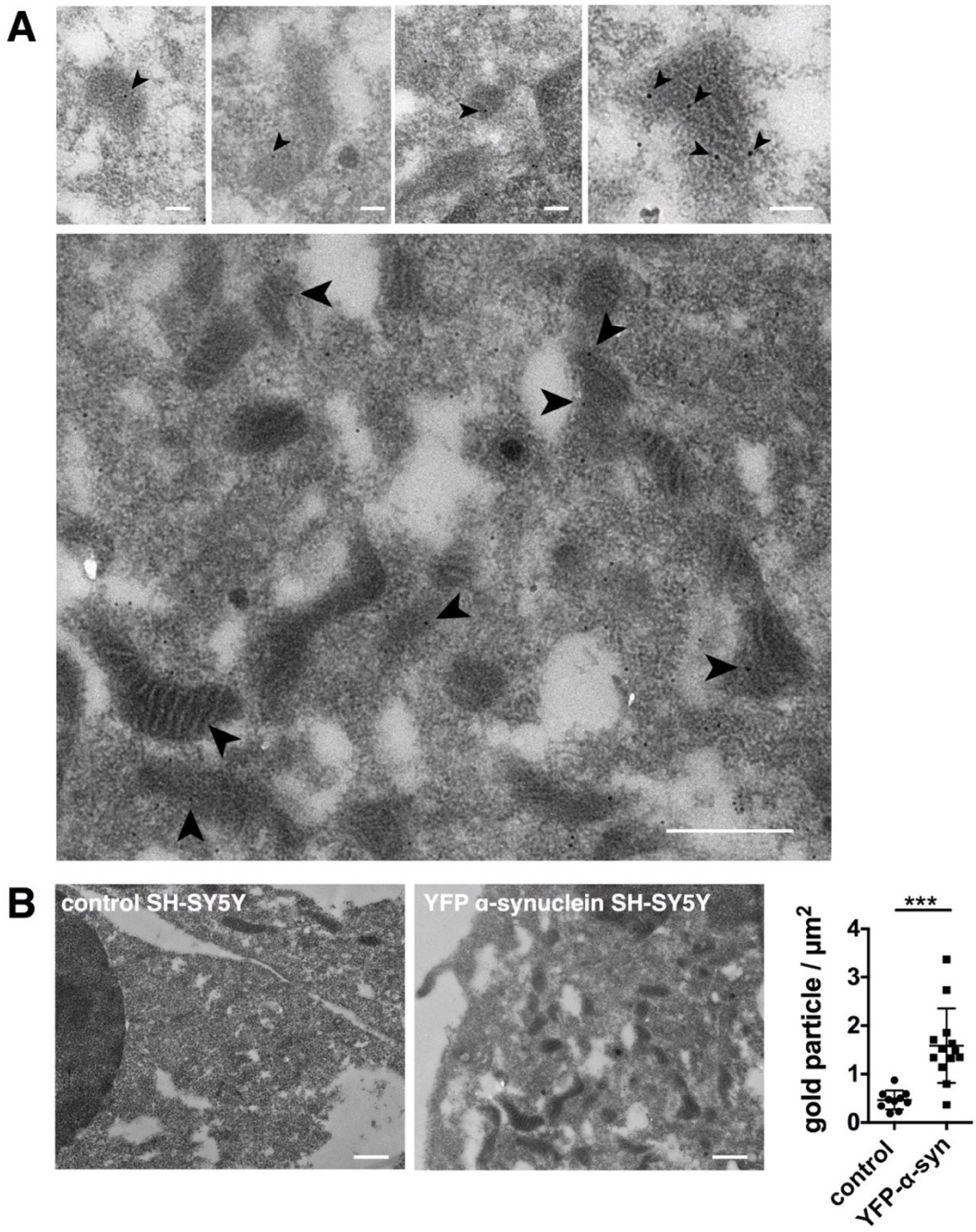

Supplementary Fig. 2. TEM of immunogold labelled YFP-alpha-synuclein, supplementary to Fig. 6A.
(A) Representative images of transmission electron microscopy (TEM) from SH-SY5Y cells overexpressing YFP-alpha-synuclein showing that alpha-synuclein is contained within mitochondria. Arrows indicate individual immunogold labelling of YFP-alpha-synuclein within mitochondria. Scale bars: 100 nm small images, 500 nm large overview image.
(B) TEM images and quantification of anti-GFP staining in control SH-SY5Y cells and SH-SY5Y cells overexpressing YFP-alpha-synuclein. Quantification of gold particles / µm2 shows that the staining is enriched in YFP-alpha-synuclein overexpressing cells and not due to unspecific background. Data are presented as mean ± SD. ***p = 0.0002 (two-tailed unpaired t-test). N = 10, 13 with n = images analyzed. Scale bars: 500 nm.